Journal of Sedimentary Research

Journal of Sedimentary Research, 2022, v. 92, 1093–1115
Research Article
DOI: 10.2110/jsr.2021.037

THE SEDIMENT BUDGET ESTIMATOR (SBE): A PROCESS MODEL FOR THE STOCHASTIC ESTIMATION OF FLUXES AND BUDGETS OF SEDIMENT THROUGH SUBMARINE CHANNEL SYSTEMS

JORIS T. EGGENHUISEN,[1] MIKE C. TILSTON,[2] CHRISTOPHER J. STEVENSON,[3] STEPHEN M. HUBBARD,[2] MATTHIEU J.B. CARTIGNY,[4] MAARTEN S. HEIJNEN,[5] JAN DE LEEUW,[1] FLORIAN POHL,[6] AND YVONNE T. SPYCHALA[7]

[1]*Faculty of Geosciences, Utrecht University, the Netherlands*
[2]*Department of Geoscience, University of Calgary, Canada*
[3]*School of Environmental Sciences, University of Liverpool, U.K.*
[4]*Departments of Earth Science and Geography, Durham University, U.K.*
[5]*Ocean and Earth Science, University of Southampton, U.K.*
[6]*School of Biological and Marine Sciences, University of Plymouth, U.K.*
[7]*Institute of Geology, Leibniz University Hannover, Germany*
e-mail: j.t.eggenhuisen@uu.nl

ABSTRACT: **Turbidity currents transport vast amounts of sediment through submarine channels onto deep-marine basin-floor fans. There is a lack of quantitative tools for the reconstruction of the sediment budget of these systems. The aim of this paper is to construct a simple and user-friendly model that can estimate turbidity-current structure and sediment budget based on observable submarine-channel dimensions and general characteristics of the system of interest. The requirements for the model were defined in the spirit of the source-to-sink perspective of sediment volume modeling: a simple, quantitative model that reflects natural variability and can be applied to ancient systems with sparse data availability. The model uses the input conditions to parameterize analytical formulations for the velocity and concentration profiles of turbidity currents. Channel cross section and temporal punctuation of turbidity-current activity in the channel are used to estimate sediment flux and sediment budget. The inherent uncertainties of geological sediment-budget estimates motivate a stochastic approach, which results in histograms of sediment-budget estimations, rather than discrete values. The model is validated against small-scale experimental turbidity currents and the 1929 Grand Banks turbidity current. The model performs within acceptable margins of error for sediment-flux predictions at these smallest and largest scales of turbidity currents possible on Earth. Finally, the model is applied to reconstruct the sediment budget related to Cretaceous slope-channel deposits (Tres Pasos Formation, Chile). The results give insight into the likely highly stratified concentration profile and the flow velocity of the Cretaceous turbidity currents that formed the deposits. They also yield estimates of the typical volume of sediment transported through the channels while they were active. These volumes are demonstrated to vary greatly depending on the geologic interpretation of the relation between observable deposit geometries and the dimensions of the flows that formed them. Finally, the shape of the probability density functions of predicted sediment budgets is shown to depend on the geological (un)certainty ranges. Correct geological interpretations of deep marine deposits are therefore indispensable for quantifications of sediment budgets in deep marine systems.**

INTRODUCTION

The rationale in studies about turbidity currents and their deposits often refers to submarine fans being the most voluminous sedimentary bodies on Earth (Middleton 1993) and turbidity currents the most prolific transport agents on the planet (Talling et al. 2012), yet no study has succeeded in presenting a process model that can be used to relate the turbidity currents responsible for the flux of sediment to the volumes of submarine fan deposits (Jobe et al. 2018). The budget of sediment transported onto submarine fans is governed by geological mechanisms that operate on thousands to millions of years involving climate, tectonics, and sea-level variations, and it is measured in cubic kilometers (km^3). The flux of sediment in turbidity currents is governed by complex particle-fluid dynamics operating on milliseconds to hours, and it is measured in cubic meters per second (m^3/s). This disparate spread in scales and types of controls makes calculation of geological sediment budgets from flow processes one of the big challenges in marine geosciences.

The source-to-sink approach to studying the entire geological chain of sediment production and transport has gained prominence in the past decade. It holistically tracks the budget of sediment from weathering of bedrock in mountainous or hilly catchment areas (the source), through the various depositional environments along the transport path, all the way to the terminal depositional sink in the deep oceans (Sømme et al. 2009a; Walsh et al. 2016). A strength of the source-to-sink approach has been that it made the ultimate simplification of the process of sediment transport, while still yielding robust and informative answers to geological problems. Sediment is simply distributed from the source to the sink, and the various

Published Online: December 2022
 1527-1404/22/092-1093

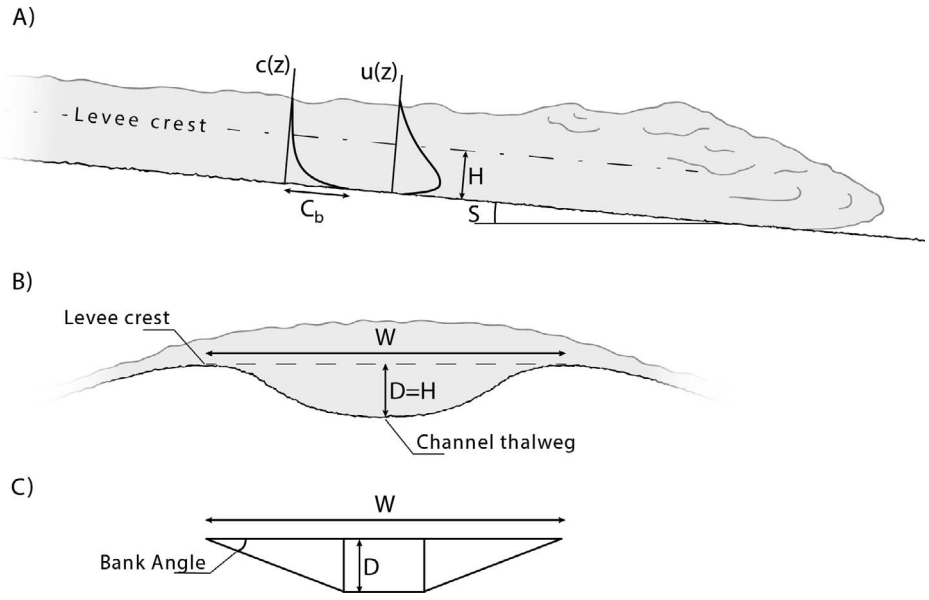

FIG. 1.—**A)** Schematic representation of the structure of a turbidity current, simplified from Altinakar et al. (1996). **B)** Schematic of the relation between channel cross section and the modeled turbidity current. **C)** Trapezoidal cross section of the model channel. The width of the rectangular thalweg section is determined after intersecting the channel margins with channel depth. **D)** The bank angle is set to 10° throughout this paper.

depositional sub-systems that are passed along the pathway (rivers, deltas, the continental shelf) act to extract a certain fraction of the available sediment budget (Paola and Martin 2012). This success may be counterintuitive when observed parallel to the development of process-based modeling efforts that seek increasingly more detailed and complex treatments of the dynamics of sediment transport (Cantero et al. 2011; Abd El-Gawad et al. 2012; Basani et al. 2014; Kneller et al. 2016). Herein we explore how turbidity-current processes can be incorporated in a source-to-sink approach without decreasing its robustness and viability. Such incorporation of process modeling into source-to-sink studies is one of the key areas for future advances suggested by Walsh et al. (2016) and Romans et al. (2016) in their reviews of the past, present, and future of the source-to-sink perspective. Geological uncertainties in source-to-sink analyses are commonly large (Sømme et al. 2009a), which means that boundary conditions for model simulations are defined as probable ranges, rather than specific values. We argue that this requires using stochastic process-modeling approaches to predictions of fluxes of sediment into deep water.

The objective of this study is to construct a simple and user-friendly model that can estimate turbidity-current parameters and sediment budgets based on observable submarine-channel parameters. This geological tool should account for natural variability and be applicable to ancient systems (Sømme and Martinsen 2017). The result is the Sediment Budget Estimator (SBE), a process-based turbidity-current model that predicts sediment budget transferred through submarine channels from the continental slope to submarine fans over geological timescales. The essence of the SBE approach is similar to the paleohydrologic "fulcrum approach" to fluvial sediment-budget estimation as proposed by (Holbrook and Wanas 2014) and applied by (Lin and Bhattacharya 2017; Sharma et al. 2017). The fulcrum method perceives a fluvial-channel cross section as the pivot between the sediment load received from the upstream domain and transmitted to a downstream domain. It analyzes the relation between the architecture of the local channel-fill deposit and the expected sediment throughput. In this paper we will describe this model approach with special emphasis on the connection between flow structures of turbidity currents, their specific geological basin setting, and the geometry of submarine channels. Consideration will be given to deep-marine concepts that can be used to constrain simulations. The model is then validated against the smallest and largest scales of sediment delivery into deep basins for which accurate dynamic data are available: laboratory-scale turbidity currents (de Leeuw et al. 2016, 2018b) and the 1929 Grand Banks turbidity current (Heezen and Ewing 1952; Kuenen 1952; Stevenson et al. 2018). Finally, the model is applied to estimate the sediment budget associated with Cretaceous submarine-channel deposits exposed in the Tres Pasos Formation in Southern Chile (Hubbard et al. 2010, 2014; Macauley and Hubbard 2013; Hubbard et al. 2020). This application demonstrates the importance of geological models derived from stratigraphic observations for sediment-budget estimates. The statistical uncertainties in sediment-budget estimates on geologic timescales can be decreased by narrowing the confidence bounds through scrutiny of the geologic record. Hence, the predictability of source-to-sink transfer of sediment to the terminal depositional sink in the deep oceans depends on the strength and confidence of geological models.

METHODOLOGY: FORMULATION OF THE TURBIDITY-CURRENT FLOW-STRUCTURE MODEL

The backbone of the SBE is formed by analytical formulations for vertical profiles of velocity, $u(z)$, and concentration, $c(z)$, in turbidity currents (Fig. 1A). These are coupled by two closure equations that relate the velocity and concentration in the flow: 1) a sediment-bypass condition that relates the shear velocity to the basal sediment concentration (Eggenhuisen et al. 2017), and 2) a conventional formulation that relates the average sediment concentration to the shear velocity (e.g., Kneller 2003; García 2008).

Velocity Profile

The velocity profile of turbidity currents has been recognized to display robust, recurring patterns (Plapp and Mitchell 1960; Stacey and Bowen 1988; Garcia and Parker 1993; Altinakar et al. 1996; Kneller et al. 1999; Kneller and Buckee 2000; Best et al. 2001; Xu et al. 2002; Gray et al. 2005; Straub et al. 2008; Islam and Imran 2010; Sequeiros et al. 2010, 2018; Xu 2011; Eggenhuisen and McCaffrey 2012; Sequeiros 2012; Cartigny et al. 2013; Cooper 2013; Pittaluga and Imran 2014; Azpiroz-Zabala et al. 2017). This robustness of the shape of the velocity profile results from the simple essential structure of turbidity currents: the bottom boundary is assumed to be a turbulent, wall-bounded shear layer; and the upper boundary is a turbulent mixing layer between the turbidity current and the ambient fluid. The velocity model developed here is therefore formed by the addition of two velocity functions: the logarithmic law of the

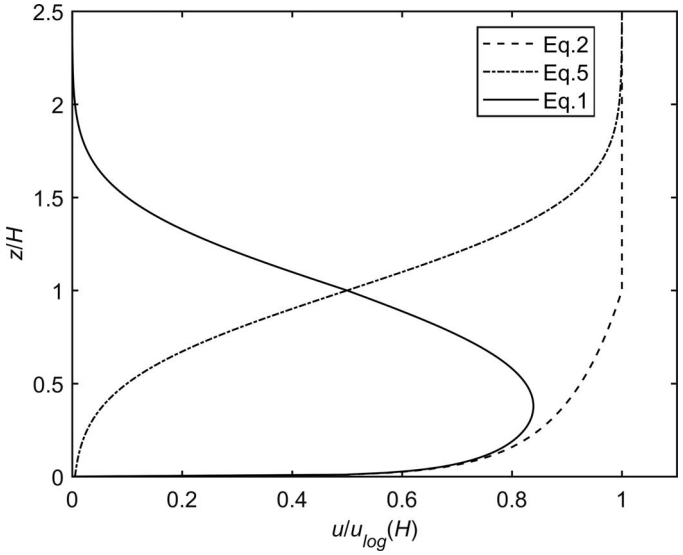

FIG. 2.—The analytical formulation for the velocity profile of turbidity currents (Eq. 1; solid line), as obtained by subtracting the plane-mixing-layer term (Eq. 5; dash-dotted line) from the logarithmic velocity (Eq. 2; dashed line). Following Kneller et al. (1999) in lieu of Altinakar et al. (1996).

wall, and a plane-mixing-layer velocity function. Several approaches have been proposed for the effective superposition of these functions (Altinakar et al. 1996; Kneller et al. 1999).

We follow the approach of Kneller et al. (1999) by assuming a logarithmic velocity profile from the bed to the flow depth, and applying a mixing layer structure throughout the water column (Fig. 2). We deviate slightly from Kneller et al. (1999), who use the "interface" between sediment-laden and clear water as the flow depth. This interface can be qualitatively observed instantaneously in turbidity currents, e.g., in pictures of experiments, but due to the multitude of turbulent mixing structures passing any one location over time it cannot be quantitatively defined in a time-averaged structure of a turbidity current, where the velocity and concentration asymptotically approach 0 with height (Garcia and Parker 1989; Islam and Imran 2010; Sequeiros et al. 2010; de Leeuw et al. 2018a). Instead, we follow Hermidas et al. (2018) by defining the elevation $z = H$ as the center of the mixing layer and the top of the logarithmic profile (Fig. 2), where z is the bed-perpendicular coordinate. This measure of flow depth (H) is equated to levee height (D) in our approach (Fig. 1B). This definition is a key aspect of the modeling strategy, and will be further justified below.

The velocity u (m/s) as a function of elevation above the bed z (m) is then

$$u(z) = u_{\log}(z) - u_{PML}(z) \tag{1}$$

The logarithmic velocity function is:

$$u_{\log}(z) = \frac{u*}{\kappa}\ln\left(\frac{z}{z_0}\right)\Big|_{z_0 \le z \le H}$$
$$u_{\log}(z) = \frac{u*}{\kappa}\ln\left(\frac{H}{z_0}\right)\Big|_{z \ge H} \tag{2}$$

where u^* is the shear velocity (m/s), κ is von Kármán's constant (0.4), z is the bed-perpendicular coordinate, and z_0 is the elevation at which the turbulent velocity profile intersects 0 m/s (Van Rijn 2011).

The nondimensional velocity distributions of plane mixing layers collapse into a universal function with the form (Champagne et al. 1976; Pope 2000):

$$f(\xi) = 1/2 erf\left(\frac{\xi}{\sigma\sqrt{2}}\right) \tag{3}$$

where σ has been analytically determined to be ≈ 0.39 (Pope 2000) and ξ is a non-dimensional coordinate perpendicular to the bed:

$$\xi = (z - z_{50})/(z_{10} - z_{90}) \tag{4}$$

The subscripts denote the elevations of the velocity percentiles, e.g., z_{50} is the z coordinate where the velocity is equal to 50% of the maximum velocity ($u_{log}(H)$). The range between z_{10} *and* z_{90} is approximated closely by H (Pope 2000).

The scaled velocity function $f(\xi)$ relates to the dimensional plane-mixing-layer velocity function as

$$u_{PML}(\xi) = u_{log}(H)[f(\xi) + 1/2] \tag{5}$$

Note that the plane mixing layer is scaled with the logarithmic velocity, not with the velocity maximum of the turbidity current (Kneller et al. 1999). The maximum velocity, as well as the elevation of the maximum velocity of the turbidity current, thus arise from the modeling, and are not constrained *a priori*. Equation 5 mathematically extends below the bed, where it asymptotically approaches 0. The residual velocity of Eq. 5 at $z = 0$ is 0.1% of $u_{log}(H)$, which is deemed insignificant for the purpose of modeling the sediment budget of submarine channel systems.

Concentration Profile

The shape of the concentration profile of many experiments is a rather similar, slightly concave exponential function (Garcia 1994; Choux et al. 2005; Islam and Imran 2010; Sequeiros et al. 2010; Tilston et al. 2015; de Leeuw et al. 2018a). The concentration function is here expressed in the simplest form of an exponential decay function:

$$c(z) = C_b e^{-kz} \tag{6}$$

where $c(z)$ is the sediment concentration at elevation z (m), C_b is the sediment concentration at the base of the flow (-), and k is a decay constant (1/m).

Closure Relations Between Variables

Sediment Bypass Closure.—Submarine channels are effective bypass conduits for sediment into deep basins (Stevenson et al. 2015; Kneller et al. 2016) that remain open conduits for most of their lifespan (Hubbard et al. 2014), such that the sediment mass eventually deposited in the channel-fill deposits at a given cross section represents only a minute part of the sediment mass transported through that cross section (Paola and Martin 2012; Stevenson et al. 2015; de Leeuw et al. 2018b). A bypass condition is therefore used here to reconstruct the characteristic sediment flux going through a channel. The bypass condition is here based on the suspension capacity parameter Γ of Eggenhuisen et al. (2017), which balances the gravitational, buoyancy, and turbulent forces acting on the suspended load. It includes universal turbulent-flow scales and material properties of the fluid and particles only. The condition $\Gamma < 1$ coincides with the complete consumption of bed-generated turbulence by sediment suspension, as observed in direct numerical simulations (Cantero et al. 2009, 2011, 2012). This oversaturated sediment condition is thought to lead to rapid deposition. The condition $\Gamma = 1$ can be used to relate the sediment concentration at the base of a bypassing turbidity current C_b to flow conditions and material properties of water and sediment (Eggenhuisen et al. 2017):

$$C_b = \frac{{u_*}^3}{140 \upsilon g R} \tag{7}$$

where υ (m^2/s) is the kinematic viscosity of water, g (m/s^2) is the acceleration

by gravity, and R (-) is the submerged relative density of quartz in water (1.65).

Parameterization of the Logarithmic Velocity Profile.—Shear velocity and z_0 are the two parameters that are needed to resolve the logarithmic velocity function (Eq. 2).

The shear velocity is estimated from the shear stress at the base of the flow due the excess weight of suspended sediment:

$$u* = \sqrt{H_r \overline{C} g R S} \tag{8}$$

where H_r is the hydraulic radius (m), which is calculated as the cross-sectional area divided by the frictional perimeter. The interface with the ambient fluid is included into the frictional perimeter here. $\bar{C}$ is the input depth-averaged sediment concentration (-), which is evaluated between the bed and $z = H$ (see Boundary Conditions, below). S is the tangent of the slope (-).

Different empirical relations have been suggested for z_0 (Garcia 2008; van Rijn 2011). In the version used here, a distinction is made between mobile and non-mobile beds, based on the ratio between the bed shear stress (τ_b) and the critical bed shear stress (τ_c) for initiation of transport of the bed material ("transport stage" *sensu* van Rijn 2011):

$$\begin{aligned} z_0 &= \frac{k_s}{30} + \frac{v}{9u^*}\Big|_{\tau_b < \tau_c} \\ z_0 &= \frac{k_s}{30} + \delta_b\Big|_{\tau_b \geq \tau_c} \end{aligned} \tag{9}$$

where k_s is the Nikuradse equivalent sand roughness (m) and δ_b is the thickness of the bedload layer (m). The Nikuradse equivalent sand roughness can be estimated from the grain size of the coarsest sediment particles on the bed (d_{90}; 90th percentile of the grain-size distribution; van Rijn 2011):

$$\begin{aligned} k_s &\approx 3d_{90}(sand) \\ k_s &\approx d_{90}(gravel) \end{aligned} \tag{10}$$

The thickness of the bedload layer is estimated as (Garcia 2008)

$$\delta_b = \frac{0.015 d_{50}[\tau_b/\tau_c]}{1 + 0.2[\tau_b/\tau_c]} \tag{11}$$

where d_{50} is the median grain size of the bed material (m). Form-roughness effects related to irregular shapes of the bed (e.g., bedforms) are not incorporated in Eq. 9.

Boundary Conditions

The structure of Equations 1–10 has been chosen such that they can now be solved when boundary-condition values are set for flow thickness H, depth-averaged sediment concentration $\bar{C}$, slope S, and characteristic bed grain size, which are all variables that deep marine geologists can estimate and debate. The probabilistic nature of the SBE will allow users to rapidly test their ideas on the confidence bounds of these parameters. It is thus not necessary to know exactly how thick characteristic turbidity currents in a system of interest are, or what their average concentration was. Rather, the model can be used to test how these parameters affect predictions of sediment fluxes and budgets. This probabilistic functionality requires the user to define a range between likely minimum and maximum values for each of the boundary conditions. These ranges are uniformly sampled by the SBE with a user-defined number of steps in between the minimum and maximum values. Equations 1–10 are solved for all combinations of each of the boundary-condition values. This can lead to tens of thousands of turbidity currents being simulated at a given cross section.

Flow Thickness Correlates to Channel Depth.—Turbidity-current thickness is often assumed to be closely related to the depth of the channel in modeling approaches (Salles et al. 2009; Abd El-Gawad et al. 2012; Arfaie et al. 2014; Basani et al. 2014; Hamilton et al. 2017; Jobe et al. 2017; Kane et al. 2017). Such assumptions of bank-full discharge are common in fluvial paleohydrology but much less straightforward in channelized turbidity currents, which may extend above the levee crest while most of the sandy sediment is bypassed in proximity to the channel floor (Hiscott et al. 1997). This key assumption will therefore be addressed in depth.

Firstly, the simple argument of scale is supported by the validity of laboratory modeling of morphodynamics of channelized turbidity currents (de Leeuw et al. 2016), which demonstrates that laboratory-size flows that are orders of magnitude smaller than real-world flows self-generate channels at dimensions similar to the flows: small turbidity currents build small channels, and large turbidity currents build large channels.

Furthermore, our morphodynamic understanding of levee building includes a self-regulatory mechanism, whereby the levees aggrade by deposition from the dilute top of the flow, causing the levee building to halt when the channel relief reaches a scale similar to that of the flow thickness (Straub and Mohrig 2008; Shumaker et al. 2018). Indeed, the variability of flow thickness with respect to channel dimensions has been argued to be small by Straub et al. (2008), who suggest that the channel form and flow scale are tuned to each other. The robustness of this self-regulatory mechanism is reflected in the successful application of the geomorphological concept of hydraulic geometry (Leopold and Maddock 1953) to submarine channels by Konsoer et al. (2013), who established that a correlative power-law relation between turbidity-current discharge and submarine-channel dimensions does exist.

Investigating the process of channelized flow in more detail, Mohrig and Buttles (2007) established experimentally that channels serve as effective conduits for turbidity currents that are 1.3 times thicker than the channel form is deep. The along-axis flow velocities are an order of magnitude higher than the cross-channel overspill velocity in such confined flows. The ratio of along-axis to cross-channel velocity rapidly decreases for partially confined flows that are thicker than 1.3 times the channel depth (Mohrig and Buttles 2007), indicating that those flows are poorly confined by the channel and rapidly spread out over the overbank area. Mohrig and Buttles (2007) use a conventional definition of flow thickness as the distance between the bed and an interface between ambient fluid and the turbidity current (H_{MB}). This interface is not defined in a time-averaged velocity profile, and falls somewhere in the top half of the mixing layer. The proposal of Hermidas et al. (2018) to define the center of the mixing layer as the flow depth (Fig. 2) is less ambiguous and more straightforward: the simple condition of $H = D$ (Fig. 1A, B) is roughly equal to the regime boundary for fully channelized flows as defined by Mohrig and Buttles (2007), because $H_{MB} = 1.3D$, and $H = D$ here.

Finally, the bypass condition based on the suspension-capacity parameter of Eggenhuisen et al. (2017) also contains a mechanism that causes channel dimensions to be attracted to a bypass state for the characteristic turbidity currents in the system. If the concentration at the base of the flow exceeds the saturation concentration, this will lead to the immediate deposition of excess sediment on the bed, until $\Gamma = 1$. This will partially fill the channel form, decreasing levee height to re-equilibrate channel dimensions with smaller characteristic turbidity currents (Shumaker et al. 2018). If the concentration falls below the saturation concentration, there is excess suspension capacity that will lead to entrainment of sediment from the channel floor. This will increase the depth and cross-sectional area of the channel to re-equilibrate with the size of larger characteristic turbidity currents.

In conclusion, a diverse suite of concepts suggests that channel size and thickness of characteristic turbidity currents are related to each other, and

TABLE 1.—*Overview of possible boundary-condition ranges and guiding principles described in the text.*

Boundary Condition	Guiding Principles			
Channel Width and Depth	Channels		Canyons	
	Bankfull Dimensions		Trimlines/Terraces	
System Slope	gentle	intermediate	steep	very steep
	0.5–1°	1–2.5°	2.5–6°	6–12°
Thalweg Grainsize (d_{50}; d_{90})	mud-rich	fine sand	medium–very coarse sand	gravel-rich
	50 μm; 200 μm	150 μm; 350 μm	500 μm; 1750 μm	1250 μm; 5000 μm
Sediment Concentration	very dilute	dilute	intermediate	high
	0.05–0.2%	0.2–0.6%	0.6–2%	2–5%
Current Duration	proximal (delta) slope	slope channels in small basins and upper continental slope	large canyons and lower continental slope	distal parts of large (≈1000 km) fans
	minutes–1 hour	1–10 hours	10 hours–2 days	days–1 week
Current Frequency	active delta slopes and tidally affected systems	shelf edge and narrow-shelf systems	distal active systems	distal abyssal plain and seismogenic supply
	weekly–monthly	seasonal	decadal	centuries–millennia
System Activity	Active part of the dominant sediment-supply cycle (kyr)		Combine with current frequency to enforce event count	

this justifies the equation of channel depth and flow thickness ($H = D$) in the first-order prediction of flow structures from channel dimensions.

Concentration: the Density of the Turbidity Current.—Robust first-order predictability of concentration magnitude through wholly process-based equations in this simplified model framework is not yet feasible. The choice is therefore made here to make the average concentration a user-defined boundary condition, rather than set it through some empirical parameters behind the scenes of the SBE. This approach at least makes the concentration uncertainty clearly defined by the user at the front end of the model. The question now arises: What are typical concentrations of turbidity currents?

Measurements of concentration profiles of real-world turbidity currents were published by Azpiroz-Zabala et al. (2017) and Simmons et al. (2020). They recorded very low depth-averaged concentrations of 0.017–0.023% in turbidity currents 48–77 m thick traveling down the Congo Canyon with a velocity of under 1 m/s. These conditions are likely to represent the slower end of the spectrum of turbidity currents in the Congo Canyon, though other measurement attempts of faster events have so far resulted in equipment failures (Khripounoff et al. 2003). Reliable measurements of average concentration are not available for such faster natural turbidity currents in other systems either. Due to the nearly complete lack of accurate concentration-profile measurements in natural flows (Wang et al. 2020), various authors have tried to estimate average concentrations by combining other variables with equations. Konsoer et al. (2013) combine friction-factor estimates with estimates of bank-full conditions that are much like the perspective set out in the previous section. This leads them to estimate a sediment-concentration range of 0.2–0.6% for a selection of channels exposed on the modern sea floor. Zeng et al. (1991) also applied friction factors to estimate sediment concentration during a turbidity current that occurred in May 1986 in the submarine channel in Bute Inlet (Canada). This turbidity current traveled at 3.6 m/s, resulting in a sediment-concentration estimate of 0.5–0.7% (Zeng et al. 1991). These values of depth-averaged concentration seem to be more representative for a broader range of active and ancient turbidity-current systems than the very dilute concentrations reported by Azpiroz-Zabala et al. (2017) for the Congo Canyon. Indeed, a compilation by Sequeiros (2012) of concentration estimates from literature leads the author to suggest that 0.45% is a typical average concentration at field scale, consistent with both the range suggested by Konsoer et al. (2013), and the estimate of Zeng et al. (1991). Finally, the Grand Banks 1929 turbidity current was the single largest turbidity-current event known to have occurred in modern times, and its size, velocity, and sediment concentration have historically been thought of as the upper limits of what is possible in oceans on Earth (Kuenen 1952). The sediment concentration was estimated to be 1.1–2.9% (Plapp and Mitchell 1960), an estimate that has recently been adjusted to 2.7–5.4% (Stevenson et al. 2018; see below). This upper concentration limit is consistent with the review by Sequeiros (2012), who suggests that the average sediment concentration of a turbidity current rarely exceeds 5%.

Based on these sources, we suggest the following broad subdivisions for the average input concentration in SBE simulations (Table 1): very dilute (0.05–0.2%), dilute (0.2–0.6%), intermediate (0.6–2%), and high (2–5%), with the dilute range advisable as a default. Interestingly, Reginald Daly arrived at likely sediment concentrations of 0.3–0.6% in his rather brilliant 1936 paper, solely by applying deductive and partially intuitive reasoning (Daly 1936). The "high" concentration class suggested here is considerably lower than the $>$ 10–15% concentration suggested for "high-density turbidity currents" by Lowe (1982). The apparent discrepancy likely arises because Lowe considered processes occurring at the bases of turbidity currents, where sediment concentrations can be much higher than the depth-averaged concentration. Indeed, observations in Monterey Canyon (Paull et al. 2018) support a model for high-density turbidity currents where a dense basal layer of up to a few meters thick, with sediment concentrations far exceeding 10%, is overlain by a thicker, dilute cloud.

The user-defined depth-averaged concentration allows evaluation of the following integral in the model workflow:

$$\overline{C}H = \int_0^\infty C_b e^{-kz} dz \tag{12}$$

Evaluation of the integral results in an expression of the decay constant k:

$$k = \frac{C_b}{\overline{C}} \frac{1}{H} \tag{13}$$

The decay constant thus depends on flow thickness, and the ratio of near-bed concentration to average concentration. This ratio often appears in modeling studies of turbidity currents (Parker et al. 1986; Halsey et al. 2017). It is the simplest measure for the degree of density stratification in the turbidity current. It approaches 2 in many experiments (Parker et al. 1987), while higher numbers have been proposed, and recently confirmed, for natural-scale flows (Azpiroz-Zabala et al. 2017; Simmons et al. 2020). Note that the concentration profile as described by Eq. 6 asymptotically approaches 0 at an indefinite elevation above the channel floor; some of the sediment declared in the two boundary conditions $\overline{C}H$ is thus actually suspended above the bank-full elevation in the exponential concentration profile. The chosen structure of Eq. 11 therefore creates a discrepancy

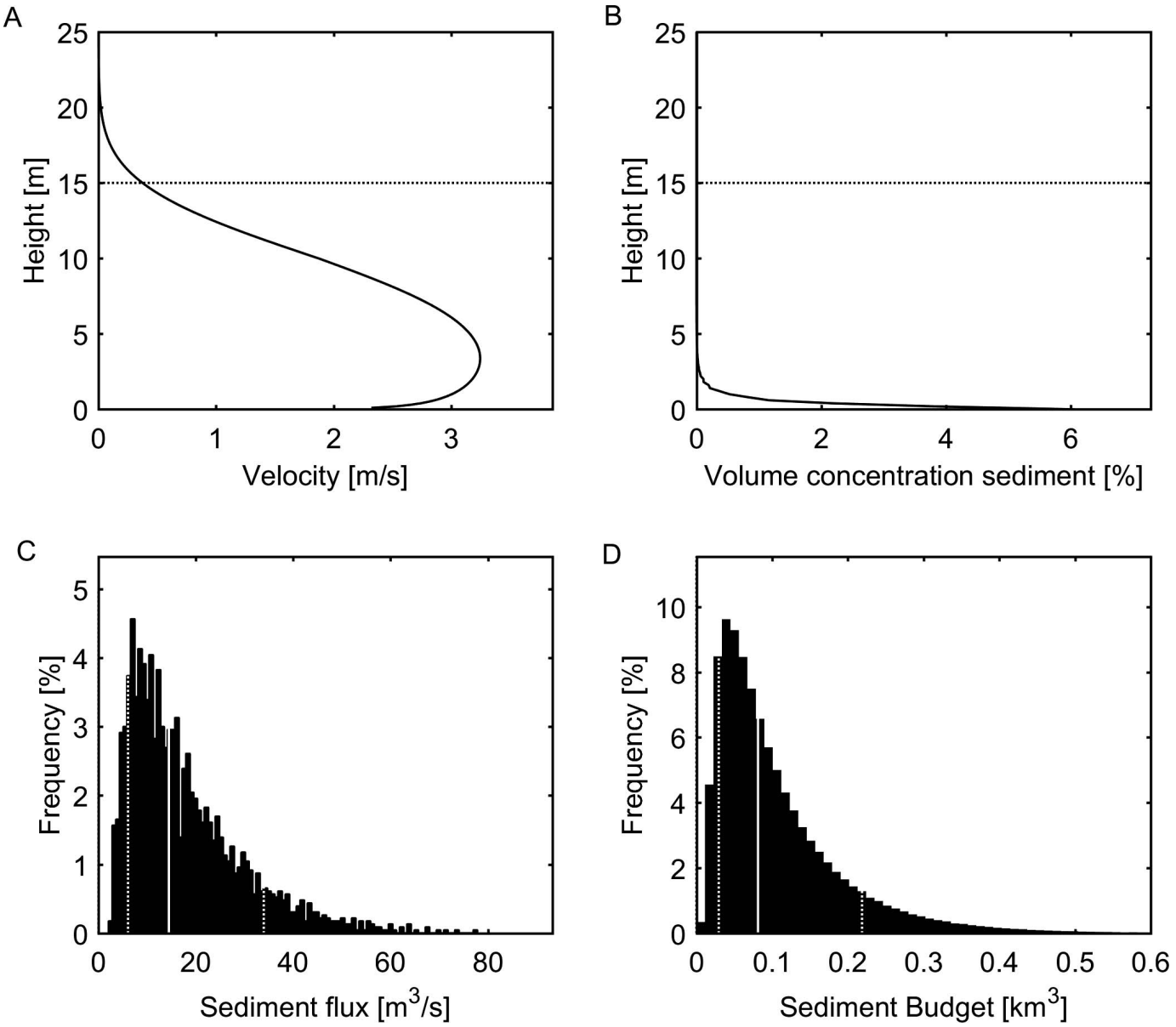

FIG. 3.—SBE default results for the base-case simulation (Table 2). **A**, **B)** Velocity and concentration profiles of a characteristic turbidity current in the base-case system. Horizontal dotted line indicates the mean input channel depth for reference. Note that the displayed example was thinner than the mean thickness. **C)** Histogram of sediment flux (m^3/s) through a characteristic channel cross section. **D)** Histogram of sediment budget of the system over a full cycle of activity. Vertical white line indicates the p_{50} of predicted sediment budgets; white dotted lines indicate p_{10} and p_{90}.

between the average concentration between the channel floor and the bankfull depth and the average of Eq. 6 between these two levels. A similar effect occurs in the more common integral approach of Ellison and Turner (1959). The magnitude of this error depends on the vertical gradient of sediment concentration near the top of the flow, and is negligible in natural currents that have low concentrations with almost no gradient at elevation H (see for example Fig. 3B).

Slope of the System.—The slope of a channel is well defined in oceanographic datasets. In subsurface systems, the slope can be estimated from seismic datasets (Shumaker et al. 2017; Beelen et al. 2019). If data does not allow the slope to be measured directly for a system, slope estimates can also be based on analogues from modern oceanography (Covault et al. 2011; Prather et al. 2016) or stratigraphic panels of outcrop systems (Johannessen and Steel 2005; Hubbard et al. 2010; Daniels et al. 2018). Compaction of clinoforms adds an extra source of uncertainty (Beelen et al. 2019) that can be taken into account when setting the confidence bounds of the slope values. Helland-Hansen et al. (2016) qualitatively grouped system styles with different steepness, and quantifications of the slope steepness have also recently been reviewed (Patruno et al. 2015; Patruno and Helland-Hansen 2018). Based on these sources, users of the SBE could use the following classes if no slope data is available for their system of interest (Table 1): gentle: 0.5–1°, intermediate: 1–2.5°, steep: 2.5–6°, very steep 6–12°. The very-steep class appears to be relevant only for steep submarine canyon systems, such as the Var Canyon (Mulder et al. 1998), the canyons in the Ebro and North Catalan margins (Amblas et al. 2006; Lastras et al. 2011), or some canyons on the North American Pacific Margin (Lee et al. 2002).

Bed Roughness.—The size of the coarsest sediment particles making up the bed determines the bed roughness, which provides a boundary condition needed to solve Eqs. 10, 9, and 2. The user is therefore required to supply an estimate of the coarse fraction of the sediment particles present on the channel thalweg. This data can be obtained from grain-size analysis of core samples obtained from the channel under investigation. It can also be taken from samples within other parts of the system when the channel body itself has not been cored, though this approach could lead to underestimation of the grain size in the channel thalweg. No grain-size samples may be available in exploration settings. Geologists will then generally be able to set likely values (e.g., Table 1) based on their understanding of the basin setting and the source area of the sediment (Reading and Richards 1994; Richards et al. 1998).

METHODOLOGY: THE SEDIMENT FLUX (m^3/s) AND BUDGET (km^3) MODULES

From Flow Structure to Sediment Flux

The sediment flux per unit width by the characteristic turbidity current can be determined by multiplying the concentration at each elevation with the corresponding velocity and integrating from the bed to an elevation some distance above the channel (Plapp and Mitchell 1960):

$$Flux_{1D} = \int_0^\infty c(z)u(z)dz \tag{14}$$

The vertical coordinate is discretized in the SBE with steps of size Δz, such that this expression can be evaluated as the dot product of the concentration and velocity profiles multiplied by the vertical step size:

$$Flux_{1D} = c(z) \bullet u(z)\Delta z \tag{15}$$

The units of this sediment flux per unit width are m^2/s. The channel cross section is here simplified to a trapezoidal shape, consisting of a flat channel-thalweg section in the middle and two channel margins on either side (Fig. 1C). The lateral channel-bank angle is user defined, but will be set to 10° throughout this paper for simplicity. The estimation of the total sediment flux through the channel cross section follows a procedure established in fluvial processes and engineering (Chang 1988): For each section in the trapezoidal cross section, we calculate a hydraulic radius, shear velocity, and velocity and concentration profiles. The resulting flux of Eq. 15 is multiplied by the section width, and the section fluxes are added to obtain the total sediment flux through the channel cross section (m^3/s). The section method can be used to calculate fluxes through more sophisticated cross-sectional channel shapes, for instance by calculating turbidity-current structures that represent more (e.g., 10) lateral channel sections in a single channel cross section. This is not pursued here, because this is deemed to only give second order improvements in predicting the sediment flux at the cost of an order-of-magnitude increase in amount of turbidity-current structures that need to be calculated. The added demand on the specificity of boundary-condition constraints, in this case the channel cross-sectional shape, is also contrary to the philosophy of the SBE.

From Sediment Flux to Sediment Budget

The sediment supply to deep-water sedimentary systems is punctuated on the time scales of events and geological cycles (Romans et al. 2016). The geological sediment budget needs to be calculated by multiplying sediment flux of the characteristic turbidity currents with the typical duration of a typical flow event, its frequency, and the (geologic) time scale of the system's activity. The sediment budget is reported by the SBE, and throughout this paper, as the volume of sediment only, *excluding* porosity of related deposits.

Turbidity-Current Duration.—Turbidity currents have been estimated in various ways from turbidite deposits to last minutes to hours (Piper et al. 1988, minimum 2 hours; Allen 1991, 20–52 minutes; Baas et al. 2000, 16–19 minutes; Jobe et al. 2012, 3–176 minutes; Jobe et al. 2017, minimum 6–12 minutes; Stevenson et al. 2018, 4–8 hours). Measurements of turbidity currents indicate that flows last minutes on proximal delta slopes (Hughes Clark 2016). The majority of monitored flows in upper canyons, however, last between 1 and 10 hours (see Talling et al. 2013 for a review). Measurements in the Congo Canyon, which is the only of the major passive-margin deep-water systems that is presently active, show that flows last up to 10 days 170 km away from the canyon head at water depths of 2000 m (Cooper 2013; Azpiroz-Zabala et al. 2017). This longer flow duration in a major canyon system is consistent with the estimate for the Pleistocene Amazon flows by Pirmez and Imran (2003). They estimated that flows lasted several days in the Pleistocene phase of activity of the Amazon fan. These measurements and estimates are in line with the suggestion by Azpiroz-Zabala et al. (2017) that turbidity-current duration is a function of distance from the source area of the flows and the stretching of flows as they transit down the system. The transit time of a flow towards a location in the basin allows the flow to stretch due to different velocities in different parts of the flow. Flows therefore last longer farther away from the source, and similarly they last longer in the distal sections of larger systems. Even the very long turbidity currents measured in the Congo Canyon can be explained in this way without invoking a sustained source mechanism (Azpiroz-Zabala et al. 2017). The timescale of duration of turbidity currents at a location can thus be estimated by dividing the distance to the source area by a characteristic stretching-velocity scale of the currents. The estimation of the stretching-velocity scale might require an iterative procedure where the SBE is initially used to reconstruct velocity profiles, which are subsequently used to evaluate the turbidity-current-duration boundary condition for sediment-budget estimates. An alternative workflow in ancient and subsurface cases, where uncertainties are inherently large, might be to set broad ranges of turbidity-current durations based on the geological setting (Table 1): minutes to 1 hour for delta slopes, hours to 10 hours for canyons in the upper continental slope and slope channels in smaller basins with steep slopes, 10 hours to a few days for larger canyons in the lower continental slope, and a few days to a week for distal parts of large ($\approx$ 1000-km-long) submarine fans.

Recurrence Time.—Recurrence times of turbidity currents are increasingly well constrained in literature (Piper and Deptuck 1997; Pirmez and Imran 2003; Xu 2011; Talling et al. 2013; Clare et al. 2014, 2016; Stevens et al. 2014; Azpiroz-Zabala et al. 2017; Allin et al. 2018; Jobe et al. 2018; Stacey et al. 2019). Much direct monitoring evidence points to a few to many tens of turbidity currents being generated each year at the top of the slope in active systems. This activity can be bundled seasonally in summer in response to meltwater hydrographs (Clare et al. 2016; Hizzett et al. 2018) or winter in response to storm activity (Xu et al. 2004; Pope et al. 2017). These very short recurrence times rapidly increase down-slope (Stevens et al. 2014; Allin et al. 2018; Stacey et al. 2019), because many turbidity currents dissipate in the slope system (Heerema et al. 2020), which is thus a staging area for sediment that is only occasionally exported all the way to the basin floor by large, fan-building turbidity currents (Jobe et al. 2018; Heijnen et al. 2022). Recurrence time of turbidity currents thus depends highly on the position in the system of interest, the mechanism that ignites these flows, and the size of the shelf itself. Consequently, flow frequency can vary from weekly to monthly or seasonal event in low-storage-capacity (short) shelves, to decadal, centennial, or even millennial-scale recurrence intervals in high-storage-capacity (broad) shelves, especially if these flows are triggered through geologic factors like the Grand Banks earthquake rather than fluvial flooding as per the Congo system. In summary (Table 1), if upper-slope

TABLE 2.—*Input parameters for the SBE simulations of a hypothetical base case, EuroSEDS experiments, and the 1929 Grand Banks turbidity current.*

		Eurotank Experiments		
	Base Case	Eurotank Experiment	Broad Ranges	1929 Grand Banks Event
Channel Width [m]	200–400	0.82 ± 10%	0.5–0.8	23000 ± 10%
Channel Depth [m]	10–20	0.072 ± 10%	0.05–0.08	201 ± 10%
System Slope [°]	1–2.5	11 ± 10%	11 ± 10%	0.45 ± 10%
Thalweg Grainsize (d_{50}; d_{90}) [*10^{-6} m]	150; 350	131; 223	131; 223	1250; 5000
Sediment Concentration [%]	0.2–0.6	15 ± 10%	15 ± 10%	Ref. 2.7–5.4 High 5.4 ± 10% Low 2.7 ± 10%
Current Duration [h]	2–4	80/3600 ± 10%	80/3600 ± 10%	4–8
Current Frequency [-/yr]	0.05–0.1	1	1	1
System Activity [kyr]	5–10	0.001	0.001	0.001

sedimentation is of most interest, the shorter recurrence times are advised as input. If sediment export to submarine fans at the base of slope is of interest, recurrence times of decades to centuries can be appropriate (see Jobe et al. 2018, for compilations of recurrence times in dated Quaternary fan systems), though evidence suggests that turbidity currents travel down major channel–levee systems, such as the Amazon, annually during periods of glacioeustatic lowstands of sea level (Piper and Deptuck 1997; Pirmez and Imran 2003). The largest millennial recurrence times seem to be restricted to abyssal-plain settings and systems where turbidity currents are triggered by rare seismic events (Clare et al. 2014).

If recurrence times for ancient examples are considered too uncertain to set as an input condition, an alternative strategy is to enforce an event count, based on stratigraphic evidence, by the combination of recurrence time and duration of system activity.

Allocyclic System Activity.—Both the duration and recurrence time of turbidity currents are aspects of the short-timescale punctuation of submarine-channel activity. Punctuation of activity also exists on longer timescales. This long timescale punctuation of activity generally relates to external, or allogenic, forcing that causes periodic attachment and detachment from the feeder systems of the submarine depositional system (e.g., shelf-edge deltas, littoral cells, or estuaries). The SBE should primarily be used to determine the sediment budget for these active phases of sediment delivery in deep marine systems.

A classic concept from sequence stratigraphy assumes that deep-water activity in sedimentary systems is highest during relative-sea-level lowstands (e.g., Posamentier and Vail 1988). This concept has been validated on various deep-water systems around the world, especially for the Pleistocene (Anderson et al. 2016; Sylvester et al. 2012). The lowstand-activity concept is most appropriate for nonglaciated, tectonically passive margins in ice-house worlds. In such lowstand-dominated systems, the duration of deep-water system activity should be set by the user to the phase within the relative-sea-level cycle during which shelf-edge deltas are present (Falivene et al. 2020). For example, Pirmez et al. (2012) document that sedimentation in the Brazos–Trinity system in the Gulf of Mexico took place mostly in the 9 kyr period from 24 to 15 ka, around the maximum sea-level lowstand in the latest Late Glacial Maximum. In the case of the Niger Delta system, Jobe et al. (2015) documented how lowstand activity lasted ≈ 30–35 kyr within an ≈ 100 kyr glacioeustatic cycle.

The effect of sea-level fluctuations on deep-water sediment delivery can be fundamentally different in steep, tectonically active systems characterized by a narrow shelf (Covault et al. 2007). Covault et al. (2007) documented how sediment derived from part of Southern California is delivered to submarine fans predominantly during sea-level highstand, when the Oceanside littoral cell is at its peak activity and generates a high supply of sediment to the La Jolla Canyon head. The Congo Canyon system is another example that does not follow the sea-level-lowstand paradigm (Khripounoff et al. 2003; Azpiroz-Zabala et al. 2017) due to the direct connection that exists between the Congo Canyon head and the Congo Estuary. These examples illustrate that strict application of a low-stand activity paradigm should be avoided if particular aspects of the basin configuration invalidate them.

Many deep-water depositional systems of interest were active in Jurassic, Cretaceous, or Paleogene times, when fluctuations of relative sea level are generally believed to have been less prominent as a forcing of sediment supply to deep-water depositional systems (Blum and Hattier-Womack 2009). In such systems climate forcing is operating through mechanisms other than glacio-eustasy, for instance by forcing sediment production and transport cycles on the continents (Carvajal and Steel 2006; Zhang et al. 2019). Interestingly, the time scale of these climatic forcings of sediment supply appears to be of order 10–100 kyr, which is similar to the glacio-eustatic lowstand reoccurrence times discussed above (Carvajal and Steel 2006; Crabaugh and Steel 2004; Grundvåg et al. 2014; Burgess and Hovius 1998; Blum and Hattier-Womack 2009). In such cases the system-activity parameter of the SBE should be set to the length of time within the climatic cycle that characterizes the phase of maximum regression of deltas to the basin margin.

SBE-RESULT STRUCTURE AND SENSITIVITY ANALYSIS

The structure of the default SBE results is illustrated with a simulation of a hypothetical system (see Table 2 for an overview of conditions). Figure 3 displays the default results of the SBE run with these input conditions. The velocity and concentration profiles of all simulated turbidity currents are stored by the SBE, but for simplicity only the profiles of a single simulated turbidity current are displayed as an example (Fig. 3A, B). This example simulation is picked from the characteristic turbidity currents whose maximum velocity is closest to the mean of all simulated maximum velocities.

The turbidity currents in this hypothetical system have a maximum velocity of ≈ 3 m/s, are highly stratified with a maximum concentration near the bed of ≈ 6%, and transport ≈ 15 m^3 of sediment every second, which amounts to ≈ 0.1 km^3 of sediment per cycle (Fig. 3). These results serve as the reference to explore: a) the sensitivity of the simulation results to uncertainty of the input conditions, and b) the response of the results to changing input conditions.

The sensitivity of the SBE to changes in input conditions is tested by reducing the uncertainty of all input variables, apart from one, to ± 1% of the mean of the base-case input range. The simulation is repeated with the uncertainty of a single different variable reinstated each time. The sediment budgets of all the simulations are displayed in order of descending spread of the predicted sediment budgets (Fig. 4), in a tornado diagram (Holbrook and Wanas 2014; Lin and Battacharya 2017). These diagrams reflect the sensitivity of the model output to the uncertainty of the variables used as input conditions. The average input sediment concentration comes out as

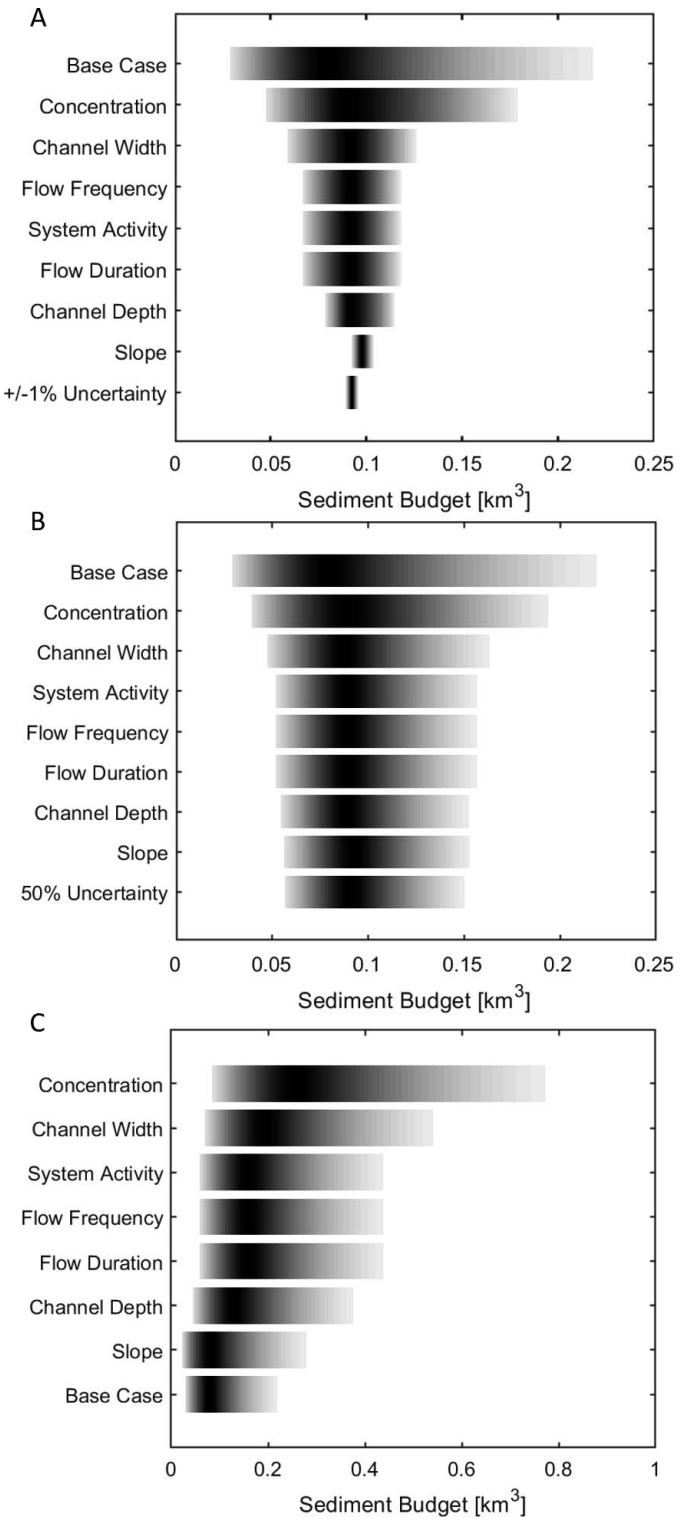

FIG. 4.—Tornado diagrams of sensitivity analyses of the SBE results. Base-case conditions are given in Table 2. **A)** Uncertainty in all variables apart from 1 is reduced to ± 1% of the mean input of the base case. Uncertainty of all variables was reduced in the "± 1% Uncertainty" scenario. **B)** Uncertainty of all variables apart from one was reduced to 50% of the uncertainty in the base case. Uncertainty of all variables was reduced in the "50% Uncertainty" scenario. **C)** Input range of a single variable was doubled compared to the base case. The gray scale changes from black for p_{50} to light gray for p_{10} and p_{90}.

the variable with most impact on the simulation results (Fig. 4A); most of the spread of the base case is maintained when all variables apart from the sediment concentration are set to range ± 1% around the mean of the base-case input. Channel width also has a relatively large impact on the spread of the sediment-budget results but is a distant second to the sediment-concentration parameter. The three temporal parameters in the SBE (flow duration and frequency, and system activity) show an identical and moderate influence on the spread of the sediment budget. Interestingly, channel depth has a smaller impact on the total uncertainty. The insensitivity to uncertainty in slope of the system is striking: the spread of predicted sediment budgets is reduced to a narrow range while the slope is still varied from 1° to 2.5° (Fig. 4A). There is thus very little benefit to be gained from increasing the confidence levels of slope estimates. This is a somewhat unexpected result due to the importance generally attributed to slope in the literature (Kneller 2003; Stevenson et al. 2015; Pohl et al. 2020).

Achieving uncertainty levels of ± 1% is unrealistic in natural turbidity-current systems. Another tornado diagram is therefore produced for which uncertainties in all variables apart from one have been reduced by 50% (Fig. 4B). This diagram confirms the sensitivity ranking of variables that was found in Figure 4A. It also shows that the spread in sediment budgets in most simulations is rather equal to that of the simulation where uncertainty in all variables has been reduced by 50% (Fig. 4B). This result indicates that it is acceptable for relatively high uncertainty to remain in one or two of the intermediate-sensitivity input parameters. There is little benefit in spending much effort on reducing that uncertainty of a single variable, because the spread in sediment budgets will remain similar even if its uncertainty is reduced by 50%. The exception to this is the input sediment concentration: even if all other variables are set to a 50% reduction of uncertainty, the spread of results does not decrease much (Fig. 4B), which again points to the importance of uncertainty about sediment concentration in turbidity currents.

As a final exercise in this section, the base case is repeated with the input range doubled for one variable at a time. The flow duration and frequency, and system activity all have a linear relation with the sediment budget, and doubling these variables results in doubling of the simulated sediment budgets (Fig. 4C). Both channel width and sediment concentration have a nonlinear effect. The concentration again has the largest impact with the predicted sediment budgets quadrupling as a result of the doubled input range. Channel depth has a subdued effect, and doubling of the slope range from 1–2.5° to 2–5°, a dramatic increase in slope within the bandwidth of natural slope angles, merely has the effect of increasing the spread of predicted sediment budgets somewhat.

VALIDATION OF THE MODEL

We validate the SBE app here with examples of the smallest-scale and largest-scale turbidity currents on Earth for which detailed data is available: laboratory turbidity currents and the 1929 Grand Banks turbidity current.

Laboratory Turbidity Currents

Boundary Conditions.—The model is first tested on Run 3 of de Leeuw et al. (2018b). This experiment was selected because it displayed the least amount of in-channel and levee deposition of all the experiments reported in that paper. It was therefore most representative of a bypassing channel, indicative of the flow-channel size equilibrium discussed above. The size of the pre-formed channel did result in a phase of initial channel deepening and widening (Fig. 5A), which indicates that the initial channel dimensions were smaller than the dimensions in equilibrium with the characteristic turbidity current initiated by de Leeuw et al. (2018b). The velocimetry data shows that channel deepening took place in the initial 40 seconds of the experiment, after which the channel thalweg stayed at a

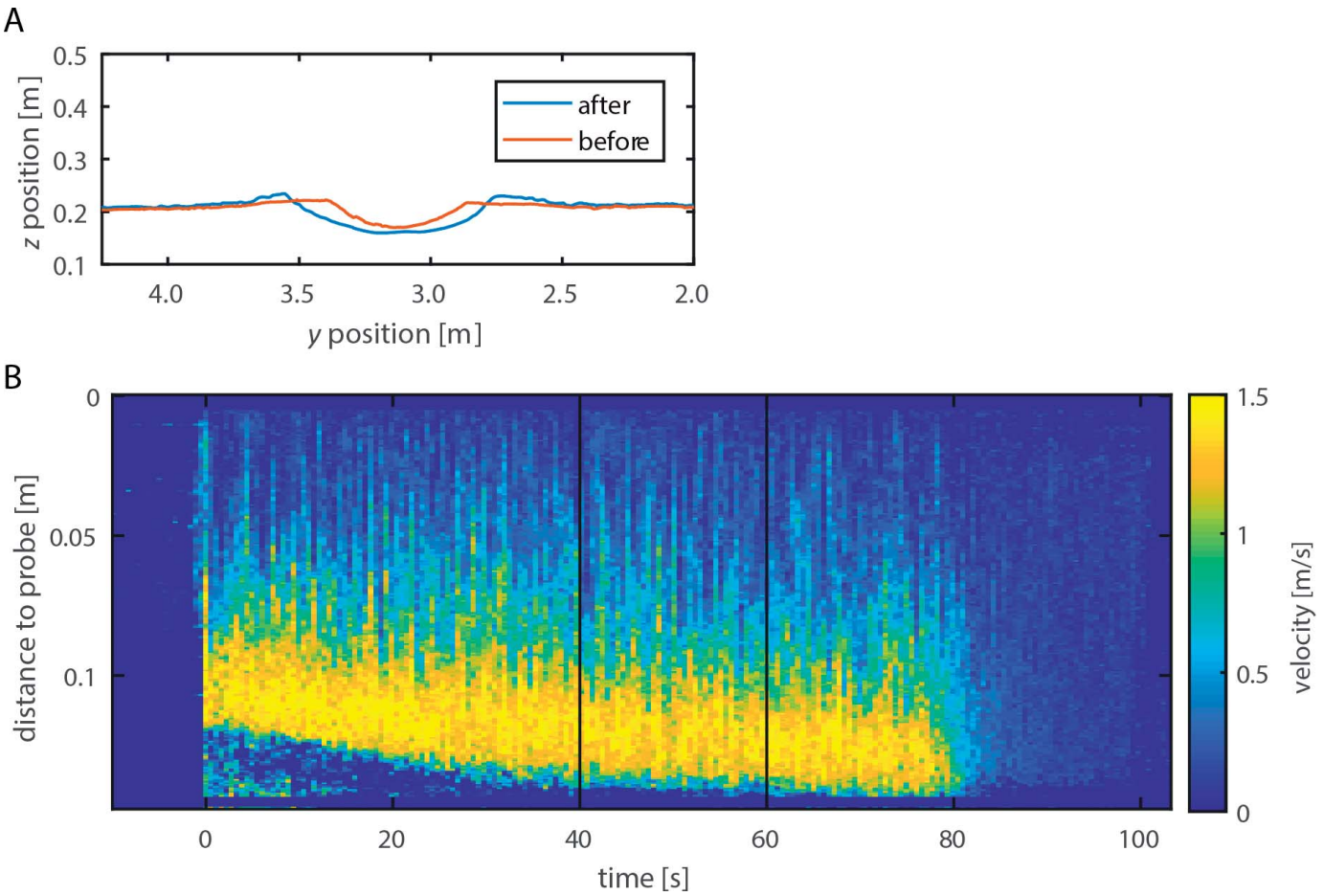

FIG. 5.—**A)** Channel cross sections measured before and after Run 3 of de Leeuw et al. (2018b). **B)** Velocity of the experimental turbidity current measured at the channel thalweg measured with an ultrasonic velocimetry profiler (UVP). The distance from the high-velocity core of the turbidity current to the UVP probe increases during the first 40 seconds of the experiment, which indicates erosion of the channel thalweg. Vertical black lines indicate the 20 s averaging window used for validation of the SBE velocity profile.

constant elevation throughout the final 40 seconds of the experiment (Fig. 5B). This is interpreted here to indicate that the initial erosive channel enlargement led to an equilibrium between the turbidity current and the channel dimensions. The channel dimensions used as input for the SBE are therefore obtained from the digital elevation model of the topography measured after the experiment. The input sediment concentration of the experiment was reported as 17% (de Leeuw et al. 2018b). The importance of the sediment concentration in the sensitivity analysis led to a reevaluation of this experimental parameter. Scrutiny of the laboratory logbook of the experiment revealed that the volume of water supplied to the mixing tank could have been as much as 0.928 m^3, and that 28 kg of sediment was recorded to remain in the pump and pipe system that supplies the mixture to the Eurotank. While the sediment in the pipes lowers the experimental sediment budget slightly, in combination with the elevated water volume it implies that the actual experimental sediment concentration could have been as low as 15% instead of the intended 17%. The full list of input conditions for the SBE are displayed in Table 2. The uncertainty ranges for the input conditions have been determined by applying an error margin of ± 10% to the best-guess values, which is appropriate for controlled sedimentology experiments.

Results.—The SBE overestimated the velocity of the experimental turbidity current; the mean of predicted velocity maxima is 50% larger than the measured velocity maximum (Fig. 6A; 2.0 m/s vs. 1.36 m/s). The predicted concentration profile has elevated concentrations near the base and decreased concentrations towards the top compared to the average input concentration (Fig. 6B). The predicted basal sediment concentration reaches the maximum granular concentration due to the high bed shear stress. The concentration profile was not measured by de Leeuw et al. (2018b), but concentrations obtained by siphoning similar turbidity currents in another setup suggest that basal sediment concentrations reach ≈ 30% (e.g., Pohl et al. 2020), not the 50+% predicted by the SBE. The experimental sediment budget falls below the range of predicted values (Fig. 6C, D). The minimum of predicted budgets is 32% higher than the experimental value; and the p_{50} of predicted budgets is a factor 2.9 times the amount of sediment pumped into the experiment.

Evaluation.—Approximately half of the predicted sediment budget falls within a factor of 2–3 of the amount of sediment pumped into the experiment. This is the expected level of accuracy of any sediment-flux estimates obtained from comparatively simple and tightly controlled open-channel flows (Chang 1988). Yet the discrepancy invites scrutiny.

Despite the experiment being well controlled, the evolution of channel shape is rather intricate due to a combination of levee aggradation, channel-thalweg incision, and channel-margin erosion (de Leeuw et al. 2018b). The overpredicted velocity and concentration profiles suggest that the final phase of the experiment represents an entrenched state of a turbidity current in a channel that is in equilibrium with a stronger current.

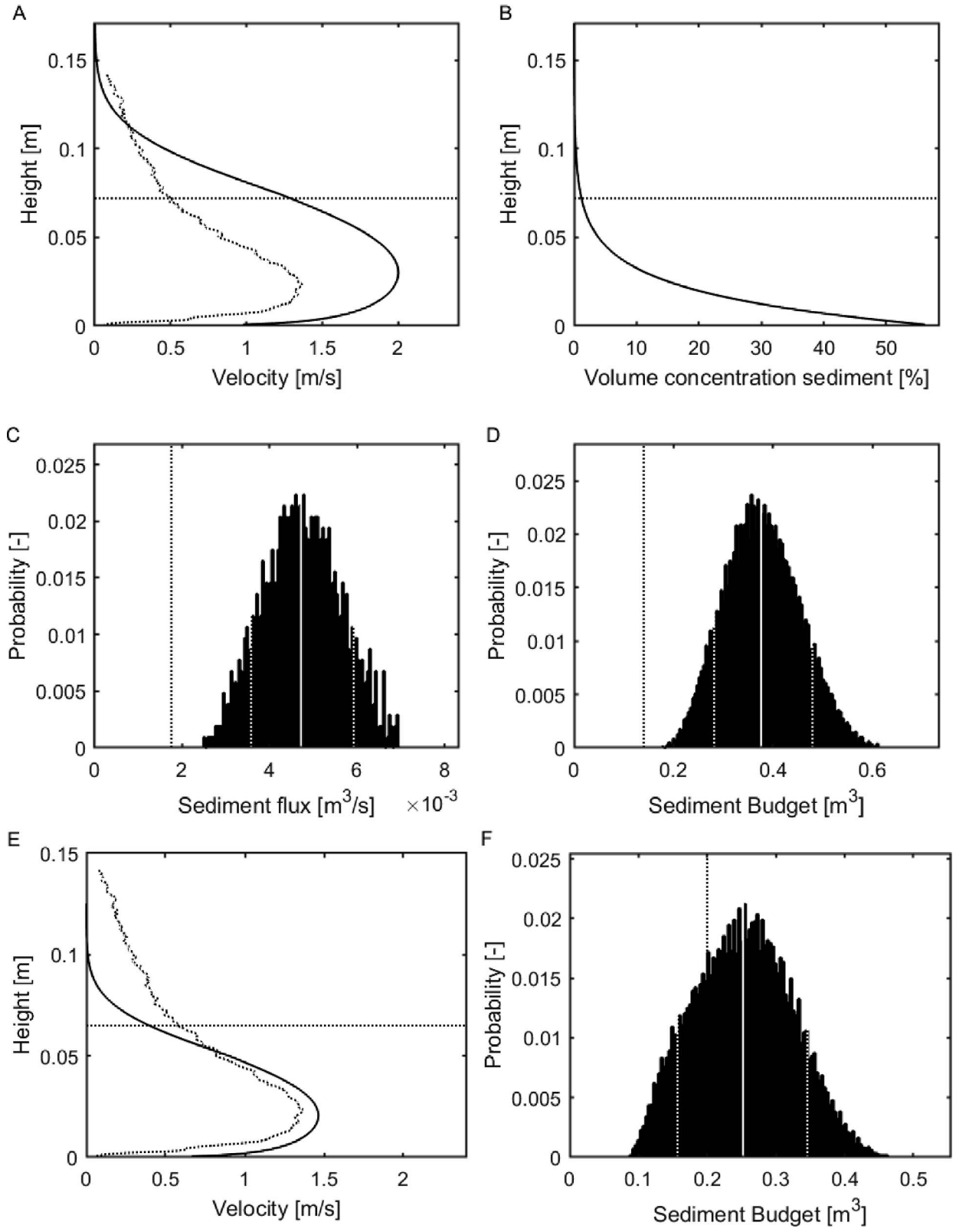

FIG. 6.—Results for the SBE simulation of Run 3 of de Leeuw et al. (2018). **A)** Velocity profile resulting from the SBE (solid line); measured velocity profile (dashed line). Horizontal dotted line indicates channel confinement depth. **B)** Concentration profile resulting from the SBE. **C)** Simulated range of sediment flux. Black dotted line indicates sediment flux of the experiment (1.9×10^{-3} m^3/s). White vertical line indicates the median of the reconstructed sediment fluxes (3.4×10^{-3} m^3/s); dotted lines indicate 10th and 90th percentiles of reconstructions. **D)** Reconstructed sediment budget. Black dotted line indicates the amount of sediment supplied to the mixing tank in preparation of Run 3 of de Leeuw et al. (2018b; 0.15 m^3). White vertical line indicates the median of the reconstructed sediment budgets (0.27 m^3); white dotted lines indicate 10th and 90th percentiles of simulated budgets.

This consideration is tested by broadening the range of channel morphologies to that of the other experiments of de Leeuw et al. (2018b) that were found to be more or less in equilibrium with the input conditions (Table 2). This increased uncertainty in representative channel shapes improves the fit between experiment and predictions. The weakest predicted velocity profile is now similar to the measured velocity profile (Fig. 6E), a considerable improvement over the narrowly constrained predictions (Fig. 6A).

Another major contributor to the original discrepancy between experiment and prediction could be the eroded sediment added to the turbidity current in excess of the budget supplied from the mixing tank, which is estimated to be ≈ 60 liters (an average of 3 cm erosion over a channel section 0.8 m wide, and 4 m long). Addition of this eroded sediment to the sediment budget raises it to ≈ 0.20 m^3, the p_{26} value of the simulated population (Fig. 6F).

The increased uncertainty improves the match between experiment and prediction. Increased precision in boundary conditions may lead to more specific results, yet such specificity should not be mistaken for increased accuracy.

Validation Against the 1929 Grand Banks Turbidity Current

Boundary Conditions.—The 1929 Grand Banks turbidity current is the largest scale event, in terms of volume of sediment transported, for which data on bathymetry, flow velocity, flow thickness, and flow composition is available (Heezen and Ewing 1952; Piper and Aksu 1987; Piper et al. 1988; Hughes Clark et al. 1990; Krastel et al. 2016; Stevenson et al. 2018). It has long been used as a testing ground for models of turbidity-current dynamics (Kuenen 1952; Plapp and Mitchell 1960; Stevenson et al. 2018). Insights from the 2015 *RV Maria S. Merian* cruise (Cruise No. MSM47; Krastel et al. 2016; Stevenson et al. 2018) are used here to constrain the SBE (Table 2). The aim of this exercise is to validate the velocity and concentration results of the SBE and establish how the range of sediment-budget estimates from the SBE relates to the estimated volume of 175–185 km^3 of the deposit that was formed on the Atlantic abyssal plain during this event (Piper and Aksu 1987; Piper et al. 1988). Specific focus is put on Transect 2 of the Eastern Valley (Stevenson et al. 2018). Approximately 70 km^3 of sediment (excluding deposit porosity; see Stevenson et al. 2018) passed through this section. The rest of the sediment forming the 175–185 km^3 deposit on the abyssal plain was transported along other flow pathways on the Grand Banks continental slope.

The boundary conditions for the simulation of the Grand Banks turbidity current are set using a combination of parameters measured in the field and reconstructed flow properties such as sediment concentration (from Stevenson et al. 2018). Channel bathymetry at Transect 2 across the Eastern Valley provides constraints on flow thickness (201 m), channel width (23,000 m), and slope (0.45°). Cable breaks across this part of the slope measured the flow speed to be 19.1 m/s (Heezen and Ewing 1952). From these data the depth-averaged sediment concentration of the flow was reconstructed between 2.7–5.4% by volume (Stevenson et al. 2018).

Results.—The SBE model shows remarkable agreement with the observed and reconstructed properties of the 1929 Grand Banks deposit and flow (Fig. 7). The velocity profile of a representative simulated flow shows a velocity maximum being slightly higher than 20 m/s, which is consistent with the velocity of 19 m/s deduced from the timing of cable breaks (Fig. 7A). The concentration profile indicates a highly stratified dense basal flow with high concentrations (> 10%) up to ≈ 25 m from the bed, overlain by a low-density cloud (Fig. 7B).

The predicted sediment flux through the channel at Transect 2 was ≈ 3 × 10^6 m^3/s (p_{50}; Fig. 7C), an order of magnitude more than the water discharge of the Amazon, which is largest river on Earth by discharge. This flux is combined with an estimated 4–8 hour flow duration (Stevenson et al. 2018). The model then predicts a p_{50} of sediment volume of 60 km^3 with a p_{10}–p_{90} range between ≈ 30 and ≈ 100 km^3 (Fig. 7D).

Evaluation.—The input sediment concentration used had a broad range from 2.7 to 5.4%, and it was shown in the general sensitivity analysis that this can impact the SBE results to a great extent (Fig. 4). To explore the validity of these results we first present a sensitivity analysis on the sediment-concentration parameter. Simulations were repeated with all parameters except that the concentration was kept the same; the concentration range was adjusted to the lower end and upper end of the estimates by Stevenson et al. (2018), each with a ± 10% uncertainty (Table 2). Low sediment concentrations of 2.7% result in flow velocities of ≈ 15 m/s (Fig. 8). In contrast, using a high-sediment-concentration condition of 4.9–5.9% results in flow velocities of ≈ 23 m/s. The low and high end of Stevenson et al.'s (2018) concentration reconstructions thus result in underestimation and overestimation of the Grand Banks velocity respectively. A concentration value midway between 2.7 and 5.4% (≈ 4%) produces flow velocities very similar to the values measured in the field (Fig. 7B). At the same time this result validates the velocity function of the SBE and the sediment-concentration reconstruction by Stevenson et al. (2018). It is worthwhile emphasizing that the sediment-concentration range was estimated by Stevenson et al. (2018) based on Chézy friction equations. This Chézy calculation output is used as an input constraint in the SBE simulation. The success of the present analysis should therefore not be seen as an independent validation against measurements only. Rather, the SBE is a corroboration of Chézy approaches (Middleton 1966; Zeng et al. 1991; Konsoer et al. 2013; Stevenson et al. 2018; Simmons et al. 2020), while modeling the effects of the mixing layer through a technique rooted in fluid mechanics (Pope 2000) rather than empirical coefficients. Stevenson et al.'s (2018) estimated flow duration of 4–8 hours was used in the SBE Grand Banks simulation (Table 2). The range of calculated sediment budgets is centered around the 70 km^3 observed in the field. Though this result seems remarkable, it adds little to the validation of the velocity and concentration scales because the SBE procedure is simply the inverse of the duration calculations performed by Stevenson et al. (2018): they estimated flow duration by dividing the sediment budget transported through the Eastern Valley by average velocity and concentration. It does illustrate, however, how the SBE quantifies the effects of remaining geologic uncertainties explicitly by reconstructing a histogram of likely sediment budgets, with a p_{10}–p_{90} range of 30–100 km^3, centered on the remarkable volume of 70 km^3 sediment transported through Transect 2 of the Eastern Valley during the Grand Banks event (Piper et al. 1988; Stevenson et al. 2018).

Validation Discussion: The Smallest and the Largest

Heezen and Ewing (1952) and Kuenen (1952) perceived the recording of the 1929 Grand Banks event by cable breaks as a turbidity-current experiment at the largest scale possible on Earth. The Eurotank experiments represent the smallest scale at which turbidity currents can be studied with natural sediments, a fluid with the viscosity of water at room temperature, and with an acceleration due to gravity of 1 *g*. The SBE performs within standard acceptable accuracy of sediment-flux predictors in these validations in isolation. It is remarkable that the SBE achieves this level of success at the smallest and largest scales possible on planet Earth, which are separated by 12 orders of magnitude, without any changes in parameterizations or the equations themselves. There is apparently no application on Earth that is outside the range of scales for the SBE, and no need to apply it outside the range for which it is established. This robustness of the SBE encourages us to seek applications of the SBE in cases where it is predictive without the possibility of validation.

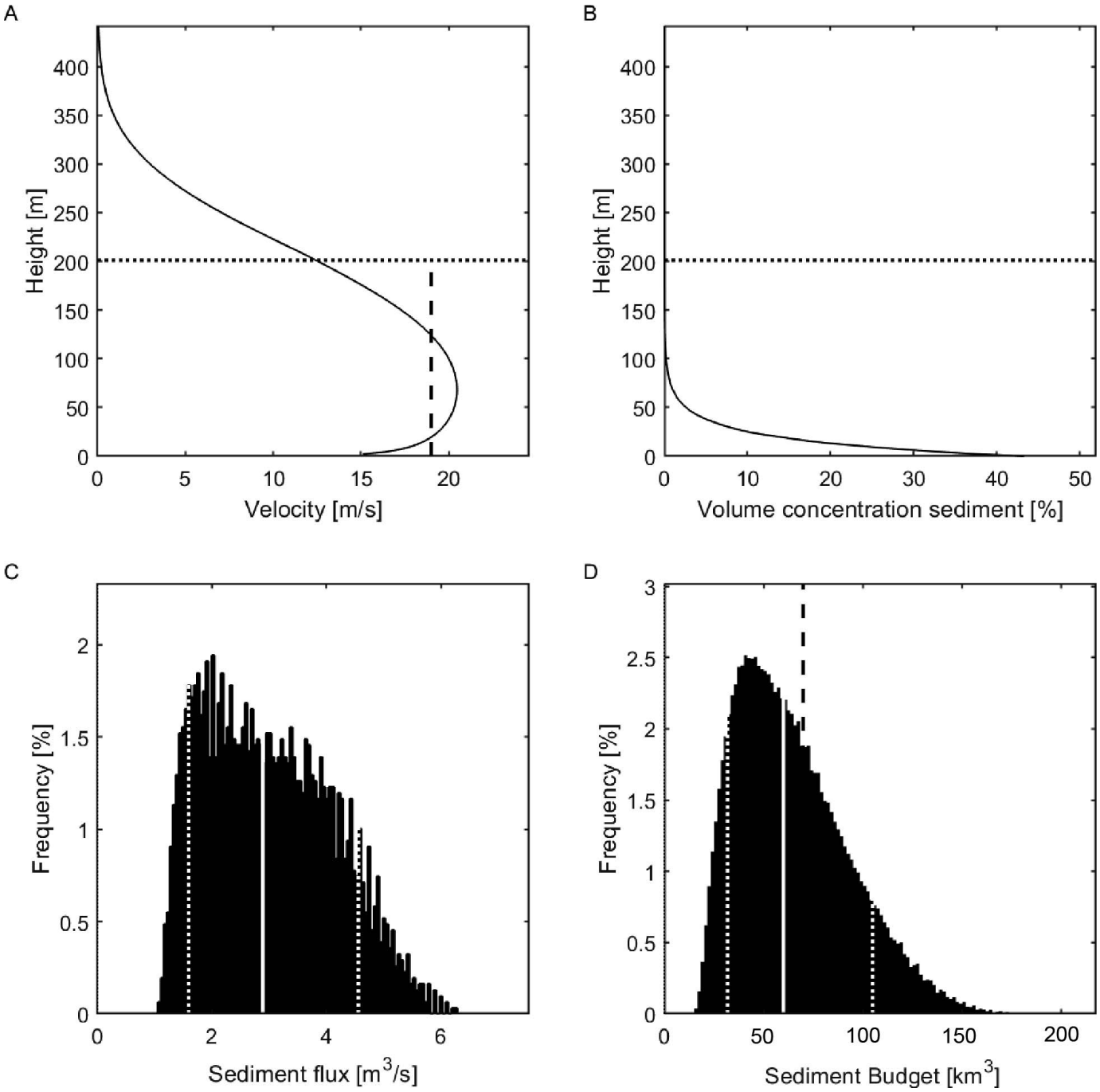

FIG. 7.—SBE results of the Grand Banks 1929 turbidity current reconstruction. **A**, **B)** Representative velocity and concentration profiles. Horizontal dotted line indicates flow thickness from Stevenson et al. (2018). Vertical dashed line indicates velocity based on the timing of cable breaks (Heezen and Ewing 1952). **C)** Sediment flux. Vertical white line indicates the p_{50} of predicted sediment flux, white dotted lines indicate p_{10} and p_{90}. **D)** Simulated sediment budget of the flow through Transect 2. Vertical white line indicates the p_{50} of predicted sediment budgets; white dotted lines indicate p_{10} and p_{90}. Vertical black dashed line indicates estimated sediment budget of the Eastern Valley (70 km^3).

APPLICATION OF THE SBE TO AN ANCIENT CHANNEL DEPOSIT IN OUTCROP

The slope channels of the Cretaceous Tres Pasos Formation (Chile) have been extensively studied in the past decade (e.g., Hubbard et al. 2010; Macauley and Hubbard 2013; Hubbard et al. 2014; Pemberton et al. 2016; Reimchen et al. 2016; Daniels et al. 2018; Hubbard et al. 2020) and provide an excellent testing ground for the application of the SBE to an ancient deep-water depositional system. One of the challenges of applying the SBE to ancient systems is making the distinction between the dimensions of channel-fill deposits and the dimensions of the conduits for the characteristic turbidity currents. Channel-fill sandstones are commonly compound deposits formed by multiple turbidity currents during alternating phases of erosion and deposition. Thus channel dimensions associated with a single turbidity current are not the same as those of the

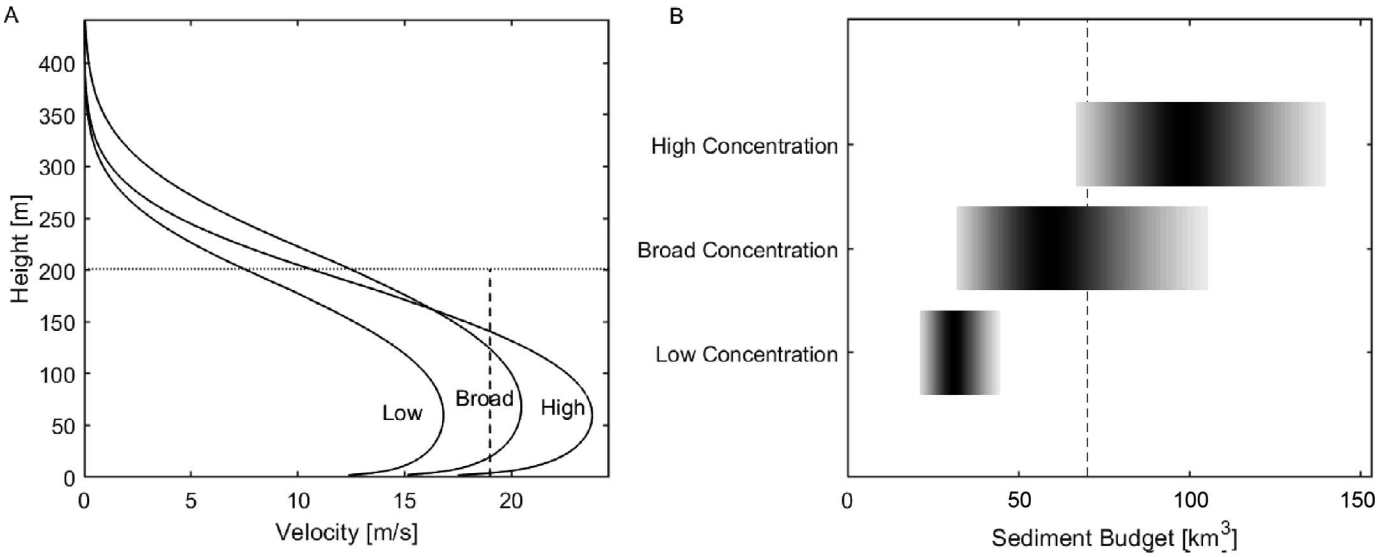

FIG. 8.—**A)** Examples of characteristic velocity profiles obtained for low-concentration estimate (slow flow), broad-concentration estimates (intermediate flow), and high-concentration estimates (fast flow) of the 1929 Grand Banks turbidity current. Vertical dashed line indicates cable-break velocity. **B)** Simulated sediment-budget ranges for the three concentration ranges (see Table 2). Gray scale changes from black at p_{50} to light gray at p_{10} and p_{90}. Vertical dashed line indicates observed 70 km^3 sediment budget.

channel fills. Hubbard et al. (2014, 2020) recognized this discrepancy and argued for using interchannel erosion surfaces to make the distinction between sediment-conduit dimensions ("story" deposit) versus those of the composite channel element. The analysis below investigates the significance of this interpretation for the projected sediment budget associated with the lifespan of a channel element. Additionally, an erroneous attribution of channel-complex dimensions, which are commonly observed in seismic data (Samuel et al. 2003; Macauley and Hubbard 2013), to the characteristic turbidity-current scale will be investigated.

Boundary Conditions

Channel-Form Dimensions.—Channel-form dimensions are estimated for the "M2" channel element, which is the focus of the recent paper by Hubbard et al. (2020). Three sets of dimensions are used as input conditions (Table 3): a) intrachannel element surfaces delineating channel story deposits have vertical and horizontal scales of 2.5–6.5 m and ≈ 200 m, respectively (Hubbard et al. 2020); b) the primary channel surface delineating the M2 channel element deposit has a vertical scale of 17 m, and is estimated to be 400 m wide (Hubbard et al. 2020); and c) channel elements are commonly grouped in channel complexes that are typically 800–1000 m wide and 30–60 m thick (Macauley and Hubbard 2013).

TABLE 3.—*Input conditions used to simulate characteristic turbidity currents at the story, element, and complex scales in the Tres Pasos Formation.*

	Scenario Story	Scenario Element	Scenario Complex
Channel Width [m]	200 ± 10%	400 ± 10%	800–1000
Channel Depth [m]	2.5–6.5	17 ± 10%	30–60
System Slope [°]	0.7–0.9	0.7–0.9	0.7–0.9
Thalweg Grainsize (d_{50}; d_{90}) [μm]	200; 400	200; 400	200; 400
Sediment Concentration [%]	0.2–0.6	0.2–0.6	0.2–0.6
Current Duration [h]	3–6	3–6	3–6
Current Frequency [-/yr]	0.1	0. 1	0.1
System Activity [kyr]	5	5	5

System Slope.—The M2 channel is part of the Figueroa clinothem (*sensu* Hubbard et al. 2010), which has an estimated paleorelief of ≈ 1000 m. Daniels et al. (2018) estimated the paleo-slope at this position in the Figueroa clinothem at 0.7–0.9°.

Grain Size.—The axial channel-fill deposits of the Tres Pasos Formation slope channels are dominated by amalgamated, thick-bedded, fine to medium-grained sandstones. Grain-size measurements on thin-section images yielded a D_{50} of 200 μm (de Leeuw 2017). The D_{90} was measured as 400 μm.

Turbidity Current Duration.—The Tres Pasos Formation contains relatively small slope channels with a length of tens of kilometers, and the flow duration is therefore set to 3–6 hours.

Turbidity Current Frequency and System Activity.—Hubbard et al. (2020) recognized evidence for approximately 500 turbidity current events in the terrace deposits on the margin of the M2 channel. For the purpose of the parameterization of the SBE input conditions, this event count is transformed into paired values of decadal recurrence times and 5 kyr system activity.

Results

From the constraints of the field data, the SBE model predicts turbidity-current structure and the sediment flux and budget for the various stratigraphic scales of channel organization. We here follow the interpretation by Hubbard et al. (2014, 2020) that the intra-element surfaces that delineate channel stories are correlated to the scale of the characteristic turbidity currents that formed the compound channel-element deposit. The structure of these characteristic turbidity currents at the channel-story scale is therefore discussed in most detail before addressing the implications of using channel-element and channel-complex scales in estimating the systems sediment flux and budget.

Turbidity-Current Structure.—Turbidity currents are simulated to flow at a maximum velocity of just over 1 m/s (Fig. 9A). The velocity maximum of the single simulation presented in this figure is located

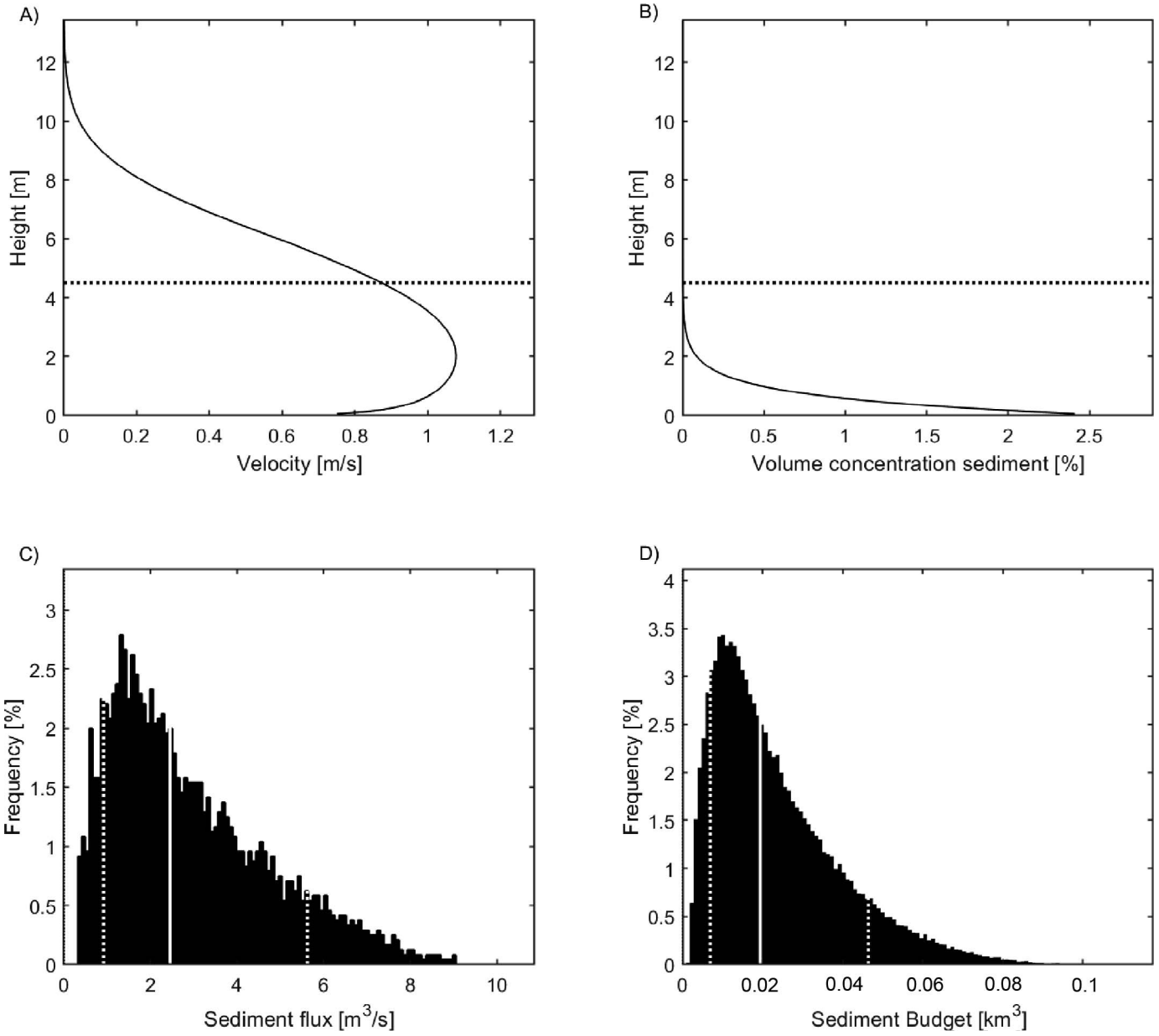

FIG. 9.—SBE results for characteristic turbidity currents related to story dimensions in Tres Pasos Formation slope channels. **A)** Velocity profile of one typical simulation; dotted line indicates mean story-surface depth. **B)** Sediment-concentration profile of one typical simulation. **C)** Histogram of calculated sediment fluxes through the channel cross section per second. Vertical white line indicates the p_{50} of predicted sediment flux; white dotted lines indicate p_{10} and p_{90}. **D)** Histogram of cumulative sediment budget of 500 characteristic turbidity currents. Vertical white line indicates the p_{50} of predicted sediment budgets; white dotted lines indicate p_{10} and p_{90}.

approximately 2 m above the bed, roughly half of the mean channel-story surface elevation. The velocity decreases until it approximates 0 m/s at 10–12 m above the channel floor.

The sediment-concentration profile displays strong stratification, with most sediment suspended near the base of the flow (Fig. 9B). The basal sediment concentration of the example simulation is 2.5% by volume, yet at the elevation of the maximum velocity (2 m) the sediment concentration has decreased to less than 0.1% by volume. The mean of the basal sediment concentrations for all 2401 simulated characteristic turbidity currents is 3.0% by volume, roughly 10 times the depth-averaged sediment concentration used as input condition (0.2–0.6% vol.).

Sediment Flux and Budget.—The simulated sediment fluxes through the channel cross section are 0.9–3–6 m^3/s (p_{10}–p_{50}–p_{90}; Fig. 9C). This amounts to a sediment budget of 0.007–0.02–0.05 km^3 (p_{10}–p_{50}–p_{90}) over the full evolution of the 500 turbidity currents that formed the channel-element deposit (Fig. 9D).

Story–Element–Complex.—The larger dimensions of the composite channel-element and channel-complex scales lead, if associated with characteristic turbidity currents, to much larger flows and sediment budgets (Fig. 10). The simulated flow velocities increase to 2.5 and 4 m/s, respectively (Fig. 10A). This combines with the much thicker column of suspended sediment to accumulate sediment budgets that are in the order

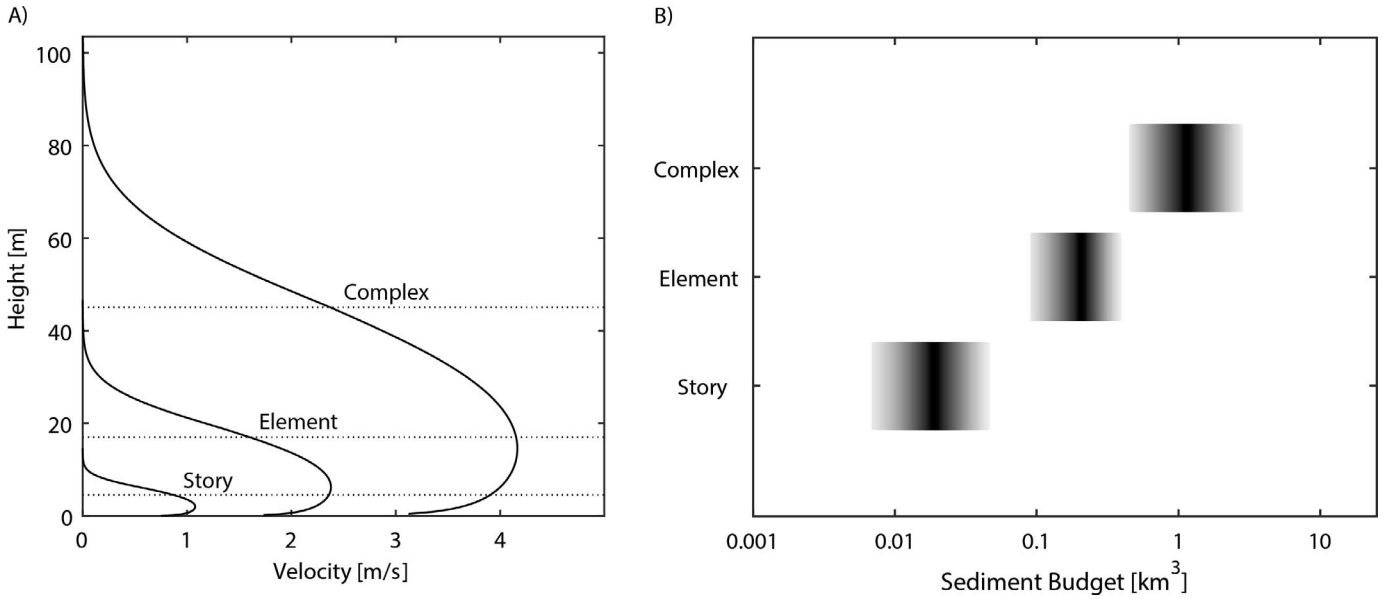

FIG. 10.—**A)** Example characteristic turbidity currents resulting from story dimensions, element dimensions, and unrealistic complex dimensions.

of 0.1 km^3 for the element-dimension simulations and 1 km^3 for the complex-dimensions simulations, compared to 0.01 km^3 simulated when story dimensions are used to simulate the characteristic turbidity currents (Fig. 10B).

Discussion of Application to an Ancient Example

Highly-Stratified Turbidity-Current Structure.—Most of the sediment in the characteristic turbidity currents simulated for the Tres Pasos Formation M2 channel is suspended near the base of the flow. The remainder of what would typically be viewed as "the turbidity current" (say from 2–12 m above the bed), is relatively devoid of sediment. This result corroborates recently emerging measurements and perspectives on the concentration structure of turbidity currents. Measurements of sediment concentration with acoustic Doppler current profilers (ADCPs) indicate that sediment concentrations in the bulk of the recorded flows are indeed very low (≈ 0.02%; Azpiroz-Zabala et al. 2017; Simmons et al. 2020). ADCPs have generally been deployed above submarine channels and canyons, to monitor turbidity currents downwards, which gives interference and resolution problems near the bed. These measurement difficulties mean that the 2-m-thick part with elevated sediment concentrations depicted in Figure 9B would typically be poorly resolved at most in ADCP data (Simmons et al. 2020). This would obscure the fact that the turbidity current is a very dilute cloud that is driven mainly by a dense basal layer (Cartigny et al. 2013; Paull et al. 2018; Simmons et al. 2020).

It is interesting to discuss here how stratification of concentration profiles is included in depth-averaged modeling workflows of turbidity currents, an approach that is more complicated than the simplified approach of the SBE. Parker (1982) proposed a simple measure for stratification in depth-averaged modeling of turbidity currents: the ratio between the near-bed sediment concentration and the depth-averaged sediment concentration, r_o, a notation that has mostly been followed by the many papers following the depth-averaged approach to modeling turbidity currents (for recent examples see Traer et al. 2012; Halsey et al. 2017; Bolla Pittaluga et al. 2018). On its first appearance, r_o was evaluated as a function of grain size with the Rouse equation for suspended-sediment concentration (Parker 1982). The Rouse equation was derived not for turbidity currents but for open-channel flow (Rouse 1937). Even though it has been shown to be a reasonable approximation for fine-grained suspended sand, and in general for the sediment suspended in the lower part of the flow, it mispredicts suspension of mud, especially in the upper part of the flow, because it neglects mixing with the ambient water in the mixing layer (Jobe et al. 2017; Eggenhuisen et al. 2019). Parker et al. (1986) dropped reliance on the Rouse equation and instead advised a value of $r_o = 1.6$, while Garcia (1994) advised $r_o = 2.0$, both based on a compilation of concentration profiles obtained from weakly-stratified, small-scale laboratory experiments. These low values for r_o are used in modeling studies to this date (Traer et al. 2012; Halsey et al. 2017; Bolla Pittaluga et al. 2018). Dorrell et al. (2014) attempted to validate depth-averaged simulations with unstratified "top-hat" concentration profiles (with r_o=1) and weakly stratified profiles against measurements of gravity currents in the Black Sea. The unsatisfactory results of their validation led Dorrell et al. (2014) to hypothesize that field-scale flows have larger degrees of stratification that are poorly represented by the stratification observed in small-scale experiments. Recent acoustic measurements of sediment concentrations in the Congo Canyon indicate that r_o was ≈ 10 in the turbidity currents reported by Azpiroz-Zabala et al. (2017) and Simmons et al. (2020). The SBE results presented here are consistent with this elevated stratification in field-scale turbidity currents compared to laboratory turbidity currents, with $r_o \approx 10$ for the Tres Pasos simulations (Fig. 7B), and $r_o \approx 11$ for the Grand Banks simulation (Fig. 9B).

Sediment Flux and Budget of the M2 Channel Element.—The simulated sediment flux through the M2 channel (Fig. 9) is comparable to the sediment flux of the turbidity currents in the Congo Canyon reported by Azpiroz-Zabala et al. (2017). The total sediment budget of the M2 channel element is comparable to the "X-channel" on the Niger slope (0.02–0.05 km^3; Jobe et al. 2018), though this was delivered to the lobe by a smaller number (20–50) of turbidity currents with a centennial recurrence time, rather than the 500 events of the M2 channel. The M2 sediment budget is smaller than the volumes of other Quarternary fans evaluated in Jobe et al. (2018), which are typically of order 1 km^3 with event counts varying from 10 to 700. This comparison shows that the reconstructed sediment flux and budget for the M2 channel are within the bandwidth of values measured in other systems, though in the lower part of this

bandwidth. This is consistent with the suggestion by Jobe et al. (2018) that smaller volumes are associated with intraslope and base-of-slope channels. A consideration of stratigraphic hierarchy could also explain the modest sediment budget predicted for the M2 channel element. Though it is not entirely clear whether lobe elements (Prélat et al. 2009) can be correlated one-to-one with a single, coeval channel element (Cullis et al. 2018), it is interesting to observe that the predicted sediment budget for the M2 channel compares very well with the volume estimates of lobe elements compiled by Prélat et al. (2010). This point will be considered further in the section below.

Story–Element–Complex–Fan.—Constraining the SBE with different hierarchical scales leads to disparate distributions of predicted sediment budgets (Fig. 10): the ranges of the three sets of predicted sediment budgets do not overlap. Each step upward in dimensions of the assumed contemporaneous channel form results in roughly an order-of-magnitude increase in predicted sediment budget. Hubbard et al. (2014, 2020) have argued extensively for associating intra-channel-element surfaces to the scale of formative turbidity-current processes based on facies analyses. The larger channel-fill deposits recognized in single channel elements are formed by a compound evolution of erosion and deposition, akin to "the fluvial valleys that never were" of Strong and Paola (2008; Hubbard et al. 2020). Association of channel-element thickness with formative turbidity current flows would lead to much thicker (17 m vs. 2.5–6.5 m; Fig. 10A) and faster flow ($\approx$ 2.5 m/s vs. $\approx$ 1 m/s; Fig. 10A), which combines to yield an order-of-magnitude larger sediment budget over the lifespan of the M2 element (Fig. 10B).

Multiple channel elements are commonly stacked consistently into channel complexes (e.g., McHargue et al. 2011; Macauley and Hubbard 2013). In our preferred interpretation, the sediment budget for channel complexes is obtained by multiplying the budget based on intra-channel surfaces (channel-story dimensions) by the typical count of elements in a complex rather than using channel-complex dimensions as inputs to SBE. Macauley and Hubbard (2013) mapped 18 channel elements in the three channel complexes that form the lower half of the Figueroa clinothem. This suggests a typical sediment budget during one channel-complex evolution of $\approx$ 0.1 km^3 (p_{50}), much less than the volumes predicted if the complex dimensions were erroneously associated with formative turbidity currents (p_{50} = 1 km^3; Fig. 10B). A similar point is made by Covault et al. (2021), who emphasize the difference in scale between the "characteristic channel width" and the much larger channel-belt width in high-sinuosity meandering submarine channels. This illustrates the consequences of erroneously relating channel-fill, channel-complex, or channel-belt dimensions to the sizes of their formative flows. It also emphasizes that careful interpretation of stratigraphy is critical for accurate estimation of primary aspects of the system, such as the order of magnitude of sand transported down-dip. This is particularly important in large-scale subsurface datasets that can lack resolution to map individual elements.

Extrapolation of the sediment budget to the entire sand-rich package of the Figueroa clinothem at the Laguna Figueroa localities (Macauley and Hubbard 2013; Hubbard et al. 2014; Pemberton et al. 2016; Hubbard et al. 2020) yields a total SBE-derived turbidity-current sediment budget of order 1 km^3. This volume would have been deposited during an unconstrained subsidiary phase within an $\approx$ 2 Myr stratigraphic interval duration (Daniels et al. 2018). The depositional body formed at this largest timescale could appropriately be called a fan. This SBE volume estimate is an entry into the suite of source-to-sink metric correlations available from the literature (Sømme et al. 2009a, 2009b). A 1 km^3 sediment volume for the Figueroa clinothem fan could correlate to a fan length of 20–150 km and a fan area of order 1000 km^2 (Sømme et al. 2009b).

GENERAL DISCUSSION

An Extra Tool in the Source-to-Sink Toolshed

Estimates of sediment budgets in submarine depositional systems can also form an inroad into a broader understanding of the setting of the system in a source-to-sink analysis (Jobe et al. 2018). An important aspect of source-to-sink analyses is that metrics obtained for different segments can be correlated to each other because regional plate tectonic and climatic conditions ensure consistency within a system (Sømme et al. 2009a, 2009b, Walsh et al. 2016). By predicting metrics of basin-floor lobes from base-of-slope channel metrics the SBE intrinsically correlates between the deep-marine segments of the chain of sediment transport. Furthermore, the reconstructed fan volume, length, and area can be used to estimate slope length (Sømme et al. 2009a, 2009b). The estimated slope length for the Tres Pasos Formation example analyzed above would be kilometers to tens of kilometers, which is consistent with the stratigraphic reconstructions by Daniels et al. (2018). Dimensions of the shelf-staging area (Sømme et al. 2009a) can be evaluated against the depositional style of coeval shelf-top delta deposits of the Dorotea Formation (Romans et al. 2011; Daniels et al. 2018). And correlated long-term deposition rates of order 10^6 t/yr (Sømme et al. 2009a) can be used to evaluate the nature of river catchment areas that supplied sediment from the Andes into the retro-arc foreland basin (Romans et al. 2011).

Sediment-budget estimates are a rapidly evolving topic in sedimentary-system science. It has been developed for the sediment budget coming from continental catchment areas over decadal timescales in the BQART model (Syvitsky and Milliman 2007; Sømme et al. 2011; Helland-Hansen et al. 2016) and for the geological sediment budget in fluvial systems using the fulcrum approach (Holbrook and Wanas 2014; Bhattacharya et al. 2016; Lin and Bhattacharya 2017; Sharma et al. 2017). Estimations with as many tools as possible are combined in an ideal source-to-sink study. Where possible, triple assessments with BQART on catchment-area budget, the fulcrum approach for the fluvial segment, and the SBE for the deep-marine segments will result in a consistency check that can confirm the source-to-sink understanding of a system.

Model Functionality and Complexity

Functionality.—The SBE is an example of simplified modeling where much of the hydraulic complexity is hidden from the intended users (marine and sedimentary geologists) because it could lie outside their immediate area of expertise. The simplicity of the model presented here allows computation of 10^4 turbidity currents within seconds on a standard computer. This makes the tool suited to consider multitudes of scenarios, resulting in the probability distribution function of sediment fluxes into the deep oceans. Also, its computational efficiency lends itself to running multiple simulations to test different geological perspectives and the overall sensitivity of the system. The benefit of such a rapid interaction is that the geologist gains immediate insight into the consequence of different geological models for the probability distribution of predicted sediment budgets. The Tres Pasos Formation evaluation shows that interpretations of stratigraphic hierarchy are a primary control on the scale of sediment-budget estimates. An even more fundamental point is made here by comparing budget histograms of simulations with different uncertainty bounds (Table 4). The second scenario represents the base case used earlier to evaluate the basic structure of the SBE results and perform a sensitivity analysis. The minimum and maximum bounds of ranges of input conditions were set to differ by a factor of 2–3 in that scenario. This resulted in a log-normal distribution of estimated sediment budgets (Figs. 3D, 11B). An overconfident geologist may ascertain uncertainty bounds of $\pm$ 10%,

TABLE 4.—*The input conditions used to illustrate the effect of scenario confidence on predicted downdip sediment volumes.*

	Scenario Confident	Scenario Base Case	Scenario Broad Uncertainty	Scenario No Geological Model
Channel Width [m]	300 ± 10%	200–400	100–500	50–1000
Channel Depth [m]	15 ± 10%	10–20	6–30	2–100
System Slope [°]	1.75 ± 10%	1–2.5	0.5–2.5	0.1–6
Thalweg Grainsize (d_{50}; d_{90}) [μm]	150; 350	150; 350	150; 350	150; 350
Sediment Concentration [%]	0.4 ± 10%	0.2–0.6	0.2–1.0	0.05–5
Current Duration [h]	3 ± 10%	2–4	2–10	0.1–240
Current Frequency [-/yr]	0.075 ± 10%	0.05–0.1	0. 03–0.15	0.001–1
System Activity [kyr]	7.5 ± 10%	5–10	2–10	0.5–1000

which is normally possible only under controlled laboratory conditions or in modern systems with high-fidelity monitoring. This overconfidence leads to sediment-budget predictions that approaches a normal distribution, closely centered around the p_{50} (Fig. 11A). A scenario with broad uncertainty (a factor 5 difference between minimum and maximum input conditions; Table 4) results in an increasing relative likelihood that the sediment budget is small, but very large values also considered a possibility (Fig. 11C). The mode and median of the predictions start to diverge strongly for this broad range in uncertainty. Finally, in the virtual absence of geological constraints (Table 4), the most likely predicted sediment budget approaches 0 km^3, while the p_{10}, p_{50}, and p_{90} explode to 20 km^3, 3×10^4 km^3, and 1×10^6 km^3 respectively, the latter being of scale comparable to the Bengal Fan sediment budget (Curray 1994). The degree of geological uncertainty is directly linked to the shape of the probability density function (PDF) of the system's sediment-budget estimates (Fig. 11). The shape of these PDFs transition into each other with growing levels of uncertainty. This implies that the distributions are in fact all realizations of a single family of PDFs such as the binomial Poisson functions, or gamma or lognormal distributions. All of these statistical families are two-parameter and one-parameter functions. The premise is then that it should be possible to parameterize the distribution of sediment budgets directly from the boundary conditions, without the need of the Monte Carlo realizations of the SBE. This mathematical exercise is not pursued herein.

The predictions of sediment budgets in the absence of a geological model were, perhaps unsurprisingly, that any amount of sediment might have gone through these channels, yet that the most likely amount converges to nothing. Process-based prediction of sediment budget is thus not possible in the absence of geological constraints on the model. This insight justifies continued efforts by the sedimentological community to try to understand the expression of turbidity-current processes in the stratigraphic record. It also underscores the need for modelers and stratigraphers to engage in integrated projects. This should motivate the research community to strive for integrated studies with research teams involving experts in both stratigraphy and sediment-transport processes.

Complexity.—While the SBE results are consistent with known cases at the largest and smallest scales, the simulated flow structures in fact differ for the different scales (Fig. 6 vs. Figs. 7 and 9). Specifically, the real-world flows are more stratified at their bases, meaning that the near-bed gradients in suspended-sediment concentration are larger in nature than in small-scale laboratory experiments. Another striking feature is that the SBE captures the similarity of scale in flow velocity between real world (Tres Pasos) and experimental flows (order 1 m/s), despite the two orders-of-magnitude difference in flow thickness. The fact that the SBE produces varying turbidity-current structures at varying scales is a sign that while it is a simple model, it is still complex enough to yield results that cannot be foreseen and that fulfill the essential requirement of any model: we can learn something new about the process from the model results.

Empirical relations obtained by fitting small-scale experimental data cannot readily be extrapolated to full field scale, because there is always the concern of extrapolating beyond the parameter space for which the relation was originally obtained. Understanding of the physical processes, however, can be based on small-scale experiments, because the equations that describe the physical process can yield different predictions at different scales. This is illustrated by the ability of the SBE to simulate strongly stratified, high-r_o turbidity currents at field scale while many of the ideas were justified from scientific studies of small-scale experiments with poorly stratified flows. It further demonstrates that the aim of an experimental study in sedimentology can, and should be, to learn more about nature, not to learn more about the laboratory. We suggest that researchers modeling turbidity currents at the full natural scale consider highly stratified flows with $r_o \approx 10$, in future work, rather than the customary weakly stratified values of 1.6–2.0. Better still, since the input conditions of the SBE are a limited subset of the boundary conditions required for depth-averaged modeling of turbidity currents, such models could *a priori* query the SBE to obtain an estimate for r_o. These considerations are an illustration of how more simple models can be used to direct more complex models to more relevant segments of their parameter space, and how model integration between simple and more complex models can improve the relevance of simulations performed.

More complex modeling workflows exist for turbidity-current research that addresses questions beyond bulk sediment budgets. It is tempting to select one of these more complex approaches in the pursuit of higher-fidelity results. However, a potential pitfall is that more intricate model systems are in practice associated with more parameters and variables, and will therefore require the user to set more intricate and precise boundary conditions, i.e., to be more knowledgeable about the system *a priori*. This is a problem especially in ancient systems, where parameters such as bathymetry can have a controlling effect on modeled turbidity currents, yet are essentially unresolved at the resolution needed for high-fidelity simulations (Aas et al. 2010). The model presented in this paper has purposely been designed with many simplifications, so that it can serve as the first, quick, check of a system's range of parameters, either as the final stage in sediment-budget estimation workflows, or ahead of more concerted modeling efforts with higher-fidelity modeling approaches.

The benefits of the simplified modeling approach of the SBE that have been emphasized in this discussion do not preclude meaningful future extensions of the model. One desirable extension could be to include physics-based modeling of the concentration profile, the shape of which is now included with a crude exponential equation; another is the incorporation of grain-size distributions in the concentration profiles. Another useful added complexity could be distinction between flow structure and sediment flux in short-duration, dense, thin, fast, frontal cells and extended (in time), dilute, quasi-steady phases that have recently been

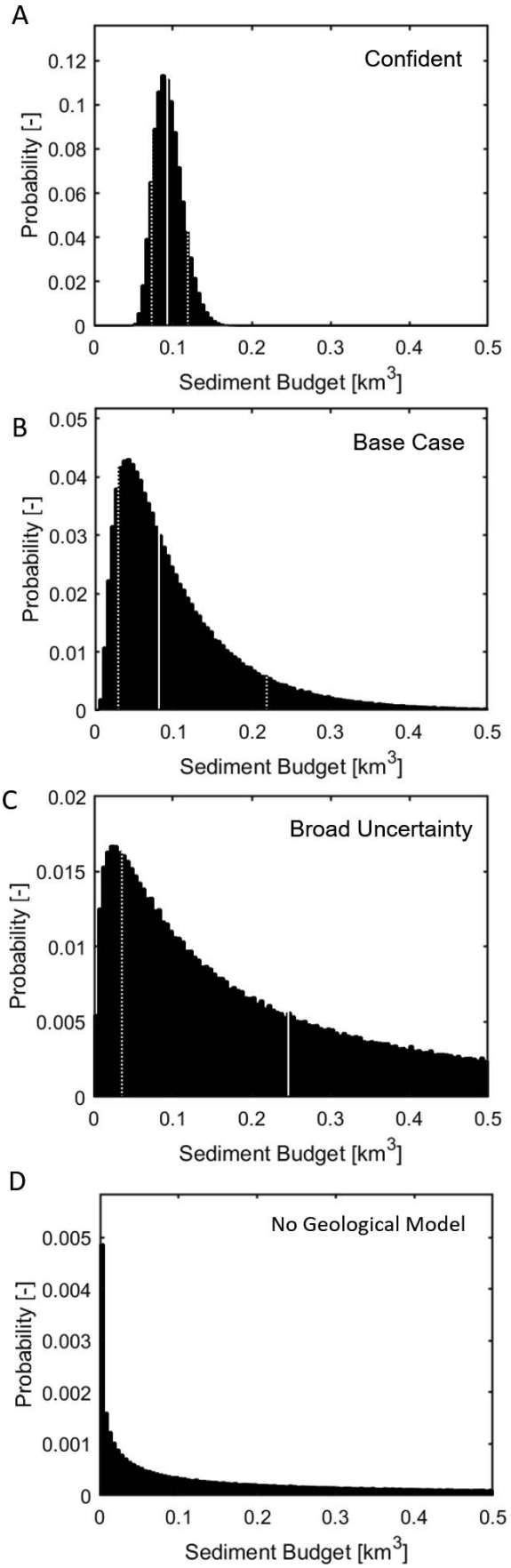

described in monitoring studies (Azpiroz-Zabala et al. 2017; Simmons et al. 2020; Wang et al. 2020). These different phases of events could have different roles in the sediment fluxes along deep-marine systems, while the initial version of the SBE presented here assumes a single, steady flow structure during the entire event duration. Such extensions of the SBE, however, should not come at the expense of the core virtues of the SBE as called for by Sømme and Martinsen (2017): a simple, quantitative model, which reflects natural variability and can be applied to ancient systems.

CONCLUSIONS

We present the Sediment Budget Estimator, a simplified, robust model that links the flow structure of turbidity currents to observable submarine-channel characteristics. The SBE uses this structure for stochastic first-order predictions of sediment fluxes and budgets in channelized turbidity-current systems. The model has been structured such that all necessary input conditions can be obtained from geological or oceanographic observations or published analogue datasets.

A sensitivity analysis reveals that fundamental uncertainty about the sediment concentration of turbidity currents has the largest impact on variability of sediment-budget predictions. Channel width also has a marked effect. Aspects of timing of turbidity currents (recurrence time, duration of individual flows, and duration of the geological activity of the system) all have linear influences on uncertainty. Channel depth is less influential, and the slope of the system has a surprisingly modest effect on the results.

The SBE is successfully validated against small-scale laboratory experiments and the 1929 Grand Banks turbidity current, with sediment budgets that differ by 12 orders of magnitude.

Application of the model to slope-channel deposits of the Cretaceous Tres Pasos Formation demonstrates the potential for paleo-sediment-budget estimates. Intra-channel-deposit surfaces with a vertical amplitude of 2.5–6.5 m are associated with formative turbidity currents. Alternative, less likely, associations between formative currents and channel-element or channel-complex scales yield budget estimates that are 1 to 2 orders of magnitude too large, respectively. The estimates of sediment budget for the lifespan of a single channel element offer an inroad into estimation of lobe element, lobe, and fan volumes. These can in turn be correlated to metrics of the slope, shelf, and catchment segments of the source-to-sink system. In such a comprehensive source-to-sink analysis the SBE can be applied together with existing sediment-budget estimators for catchment areas and fluvial systems, such as BQART and the fulcrum approach for fluvial paleohydrology.

Application of the SBE to submarine channels and their deposits in modern sea-floor settings, geological outcrops of ancient systems, and subsurface datasets will enable first-order flux and budget predictions and reconstructions of sediment and other phases.

SUPPORTING MATERIAL

The Matlab scripts that constitute the Sediment Budget Estimator have been published on Github (Eggenhuisen and Tilston 2022): https://github.com/JorisEggenhuisen/SBE. Input conditions for the simulations discussed in this paper are supplied in the same repository.

←

FIG. 11.—Sediment-budget histograms for scenarios with decreasing confidence of interpretation. Vertical white line indicates the p_{50} of predicted sediment budgets, white dotted lines indicate p_{10} and p_{90}. **A)** Confident levels of uncertainty with ± 10% ranges around a mean estimates of input conditions. **B)** The base-case scenario with factor 2–3 differences between minimum and maximum inputs. **C)** Broad uncertainty with a factor 5 difference between minimum and maximum inputs. **D)** Sediment-budget predictions in the absence of a specific geological model.

ACKNOWLEDGMENTS

JTE, MT, FP, JdL, and YS acknowlegde funding of the EuroSEDS project by NWO (grant NWO-864.13.006), ExxonMobil, Shell, and Equinor.

Discussions with Michal Janocko helped direct the functionality of the SBE at an early stage.

The participants of the Utrecht University MSc course Dynamics of Sedimentary Systems (2018–2021) are gratefully acknowledged for testing the SBE. Their course work pointed out the bugs and benefits of the SBE. Their collective success in using the SBE to constrain sediment budgets in diverse deep-water systems has provided the necessary motivation to carry this manuscript to completion. Reviewers Zane Jobe and Oriol Falivene, and Associate Editor Jake Covault, provided constructive comments that helped us improve our paper.

REFERENCES

Aas, T.E., Howell, J.A., Janocko, M., and Jackson, C.A.L., 2010, Control of Aptian palaeobathymetry on turbidite distribution in the Buchan Graben, Outer Moray Firth, Central North Sea: Marine and Petroleum Geology, v. 27, 412–434.

Abd El-Gawad, S., Cantelli, A., Pirmez, C., Minisini, D., Sylvester, Z., and Imran, J., 2012, Three-dimensional numerical simulation of turbidity currents in a submarine channel on the seafloor of the Niger Delta slope: Journal of Geophysical Research, v. 117, no. C05026.

Allen, J.R.L., 1991, The Bouma division A and the possible duration of turbidity currents: Journal of Sedimentary Petrology, v. 61, p. 291–295.

Allin, J.R., Hunt, J.E., Clare, M.A., and Talling, P.J., 2018, Eustatic sea-level controls on the flushing of a shelf-incising submarine canyon: Geological Society of America, Bulletin, v. 130, p. 222–237.

Altinakar, M.S., Graf, W.H., and Hopfinger, E.J., 1996, Flow structure in turbidity currents: Journal of Hydraulic Research, v. 34, p. 713–718.

Amblas, D., Canals, M., Urgeles, R., Lastras, G., Liquete, C., Hughes-Clarke, J.E., Casamor, J.L., and Calafat, A.M., 2006, Morphogenetic mesoscale analysis of the northeastern Iberian margin, NW Mediterranean Basin: Marine Geology, v. 234, p. 3–20.

Anderson, J.B., Wallace, D.J., Simms, A.R., Rodriguez, A.B., Weight, R.W.R., and Taha, Z.P., 2016, Recycling sediments between source and sink during a eustatic cycle: systems of late Quaternary northwestern Gulf of Mexico Basin: Earth-Science Reviews, v. 153, p. 111–138.

Arfaie, A., Burns, A.D., Dorrell, R.M., Eggenhuisen, J.T., Ingham, D.B., and McCaffrey, W.D., 2014, Optimised mixing and flow resistance during shear flow over a rib roughened boundary: International Communications in Heat and Mass Transfer, v. 107, p. 141–147.

Azpiroz-Zabala, M., Cartigny, M.J.B., Talling, P.J., Parsons, D.R., Sumner, E.J., Clare, M.A., Simmons, S.M., Cooper, C., and Pope, E.L., 2017, Newly recognized turbidity current structure can explain prolonged flushing of submarine canyons: Science Advances, v. 3, no. e1700200.

Baas, J.H., van Dam, R.L., and Storms, J.E.A., 2000, Duration of deposition from decelerating high-density turbidity currents: Sedimentary Geology, v. 136, p. 71–88.

Basani, R., Janocko, M., Cartigny, M.J.B., Hansen, W.M., and Eggenhuisen, J.T., 2014, MassFLOW-3D as a simulation tool for turbidity currents: some preliminary results, *in* Martinius, A.W., Ravnås, R., Howell, J.A., Steel, R.J., and Wonham, J.P., eds., From Depositional Systems to Sedimentary Successions on the Norwegian Continental Margin: International Association of Sedimentologists, Special Publication 46, p. 587–608.

Beelen, D., Jackson, C.A.L., Patruno, S., Hodgson, D.M., and Trabucho Alexandre, J., 2019, The effects of differential compaction on clinothem geometries and shelf-edge trajectories, Geology, v. 47, p. 1011–1014.

Best, J.L., Kirkbride, A.D., and Peakall, J., 2001, Mean flow and turbulence structure of sediment-laden gravity currents: new insights using ultrasonic Doppler velocity profiling, *in* McCaffrey, W.D., Kneller, B.C., and Peakall, J., eds., Particulate Gravity Currents: International Association of Sedimentologists, Special Publication 31, p. 159–172.

Bhattacharya, J.P., Copeland, P., Lawton, T.F., and Holbrook, J., 2016, Estimation of source area, river paleo-discharge, paleoslope, and sediment budgets of linked deep-time depositional systems and implications for hydrocarbon potential: Earth-Science Reviews, v. 153, p. 77–110.

Blum, M.D., and Hattier-Womack, J., 2009, Climate change, sea-level change, and fluvial sediment supply to deepwater depositional systems, *in* Kneller, B., Martinsen, O.J., and McCaffrey, W.D., eds., External Controls on Deep-Water Depositional Systems: SEPM, Special Publication 92, p. 15–39.

Bolla Pittaluga, M., Frascati, A., and Falivene, O., 2018, A gradually varied approach to model turbidity currents in submarine channels: Journal of Geophysical Research, Earth Surface, v. 123, p. 80–96.

Burgess, P.M., and Hovius, N., 1998, Rates of delta progradation during highstands: consequences for timing of deposition in deep-marine systems: Journal of the Geological Society, v. 155, p. 217–222.

Cantero, M.I., Balachandar, S., and Parker, G., 2009, Direct numerical simulation of stratification effects in a sediment-laden turbulent channel flow: Journal of Turbulence, v. 10, p. 37–41.

Cantero, M.I., Cantelli, A., Pirmez, C., Balachandar, S., Mohrig, D., Hickson, T.A., Yeh, T., Naruse, H., and Parker, G., 2011, Emplacement of massive turbidites linked to extinction of turbulence in turbidity currents: Nature Geoscience, v. 5, p. 42–45.

Cantero, M.I., Shringarpure, M., and Balachandar, S., 2012, Towards a universal criteria for turbulence suppression in dilute turbidity currents with non-cohesive sediments: Geophysical Research Letters, v. 39, no. L14603.

Cartigny, M.J.B., Eggenhuisen, J.T., Hansen, E.W.M., and Postma, G., 2013, Concentration-dependent flow stratification in experimental high-density turbidity currents and their relevance to turbidite facies models: Journal of Sedimentary Research, v. 83, p. 1047–1065.

Carvajal, C.R., and Steel, R.J., 2006, Thick turbidite successions from supply-dominated shelves during sea-level highstand: Geology, v. 34, p. 665–668.

Champagne, F.H., Pao, Y.H., and Wygnanski, I.J., 1976, On the two-dimensional mixing region: Journal of Fluid Mechanics, v. 74, p. 209–250.

Chang, H.H., 1988, Fluvial Processes in River Engineering: Melbourne, Florida, Krieger Publishing, 446 p.

Choux, C.M.A., Baas, J.H., McCaffrey, W.D., and Haughton, P.D.W., 2005, Comparison of spatio–temporal evolution of experimental particulate gravity flows at two different initial concentrations, based on velocity, grain size and density data: Sedimentary Geology, v. 179, p. 49–69.

Clare, M.A., Talling, P.J., Challenor, P., Malgesini, G., and Hunt, J., 2014, Distal turbidites reveal a common distribution for large (>0.1 km^3) submarine landslide recurrence: Geology, v. 42, p. 263–266.

Clare, M.A., Hughes Clarke, J.E., Talling, P.J., Cartigny, M.J.B., and Pratomo, D.G., 2016, Preconditioning and triggering of offshore slope failures and turbidity currents revealed by most detailed monitoring yet at a fjord-head delta: Earth and Planetary Science Letters, v. 450, p. 208–220.

Cooper, C., 2013, Turbidity Current Measurements in the Congo Canyon: Offshore Technololy Conference, 23992.

Covault, J.A., Normark, W.R., Romans, B.W., and Graham, S.A., 2007, Highstand fans in the California borderland: the overlooked deep-water depositional systems: Geology, v. 35, p. 783–786.

Covault, J.A., Fildani, A., Romans, B.W., and McHargue, T., 2011, The natural range of submarine canyon-and-channel longitudinal profiles: Geosphere, v. 7, p. 313–332.

Covault, J.A., Sylvester, Z., Ceyhan, C., and Dunlap, D.B., 2021, Giant meandering channel evolution, Campos deep-water salt basin, Brazil: Geosphere, v. 17, p. 1869–1889.

Crabaugh, J.P., and Steel, R.J., 2004, Basin-floor fans of the Central Tertiary Basin, Spitsbergen: relationship of basin-floor sand-bodies to prograding clinoforms in a structurally active basin, *in* Lomas, S.A., and Joseph, P., eds., Confined Tutbidite Systems: Geological Society of London, Special Publication 222, p. 187–208.

Cullis, S., Colombera, L., Patacci, M., and McCaffrey, W.D., 2018, Hierarchical classifications of the sedimentary architecture of deep-marine depositional systems: Earth-Science Reviews, v. 179, p. 38–71.

Curray, J.R., 1994, Sediment volume and mass beneath the Bay of Bengal: Earth and Planetary Science Letters, v. 125, p. 371–383.

Daly, R.A., 1936, Origin of Submarine "Canyons": American Journal of Science, v. 31, p. 401–420.

Daniels, B.G., Auchter, N.C., Hubbard, S.M., Romans, B.W., Matthews, W.A., and Stright, L., 2018, Timing of deep-water slope evolution constrained by large-n detrital and volcanic ash zircon geochronology, Cretaceous Magallanes Basin, Chile: Geological Society of America, Bulletin, v. 130, p. 438–454.

de Leeuw, J., 2017, The sedimentary record of submarine channel morphodynamics [Ph.D. Thesis]: Utrecht University, 149 p.

de Leeuw, J., Eggenhuisen, J.T., and Cartigny, M.J.B., 2016, Morphodynamics of submarine channel inception revealed by new experimental approach: Nature Communications, v. 7, no. 10886.

de Leeuw, J., Eggenhuisen, J.T., and Cartigny, M.J.B., 2018a, Linking submarine channel–levee facies and architecture to flow structure of turbidity currents: insights from flume tank experiments: Sedimentology, v. 65, p. 931–951.

de Leeuw, J., Eggenhuisen, J.T., Spychala, Y.T., Heijnen, M.S., Pohl, F., and Cartigny, M.J.B., 2018b, Sediment volume and grain-size partitioning between submarine channel–levee systems and lobes: an experimental study: Journal of Sedimentary Research, v. 88, p. 777–794.

Dorrell, R.M., Darby, S.E., Peakall, J., Sumner, E.J., Parsons, D.R., and Wynn, R.B., 2014, The critical role of stratification in submarine channels: implications for channelization and long runout of flows: Journal of Geophysical Research, Oceans, v. 119, p. 2620–2641.

Eggenhuisen, J.T., and McCaffrey, W.D., 2012, The vertical turbulence structure of experimental turbidity currents encountering basal obstructions: implications for vertical suspended sediment distribution in non-equilibrium currents: Sedimentology, v. 59, p. 1101–1120.

Eggenhuisen, J.T., and Tilston, M.C., 2022, Sediment Budget Estimator for deep marine depositional systems (1.0.0): Zenodo, doi:10.5281/zenodo.6635519.

Eggenhuisen, J.T., Cartigny, M.J.B., and de Leeuw, J., 2017, Physical theory for near-bed turbulent particle suspension capacity: Earth Surface Dynamics, v. 5, p. 269–281.

Eggenhuisen, J.T., Tilston, M.C., Leeuw, J., Pohl, F., and Cartigny, M.J.B., 2019, Turbulent diffusion modelling of sediment in turbidity currents: an experimental validation of the Rouse approach: The Depositional Record, v. 6, p. 203–216.

Ellison, T.H., and Turner, J.S., 1959, Turbulent entrainment in stratified flows: Journal of Fluid Mechanics, v. 6, p. 423–448.

Falivene, O., Prather, B.E., and Martin, J., 2020, Quantifying sand delivery to deep water during changing sea-level: numerical models from the Quaternary Brazos Icehouse continental margin: Basin Research, v. 32, p. 1711–1733.

Garcia, M.H., 1994, Depositional turbidity currents laden with poorly sorted sediment: Journal of Hydraulic Engineering, v. 120, p. 1240–1263.

Garcia, M.H., 2008, Sedimentation Engineering: American Society of Civil Engineers, 1132 p.

Garcia, M., and Parker, G., 1993, Experiments on the entrainment of sediment into suspension by a dense bottom current: Journal of Geophysical Research, v. 98, p. 4793–4807.

Garcia, M., and Parker, G., 1989, Experiments on hydraulic jumps in turbidity currents near a canyon-fan transition: Science, v. 245, p. 393–396.

Gray, T.E., Alexander, J., and Leeder, M.R., 2005, Quantifying velocity and turbulence structure in depositing sustained turbidity currents across breaks in slope: Sedimentology, v. 52, p. 467–488.

Grundvag, S.-A., Johannessen, E.P., Helland-Hansen, W., and Plink-Bjorklund, P., 2014, Depositional architecture and evolution of progradationally stacked lobe complexes in the Eocene Central Basin of Spitsbergen: Sedimentology, v. 61, p. 535–569.

Halsey, T.C., Kumar, A., and Perillo, M.M., 2017, Sedimentological regimes for turbidity currents: depth-averaged theory: Journal of Geophysical Research, Oceans, v. 122, no. C012635.

Hamilton, P., Gaillot, G., Strom, K., Fedele, J., and Hoyal, D., 2017, Linking hydraulic properties in supercritical submarine distributary channels to depositional-lobe geometry: Journal of Sedimentary Research, v. 87, p. 935–950.

Heerema, C.J., Talling, P.J., Cartigny, M.J., Paull, C.K., Bailey, L., Simmons, S.M., Parsons, D.R., Clare, M.A., Gwiazda, R., Lundsten, E., Anderson, K., Maier, K.L., Xu, J.P., Sumner, E.J., Rosenberger, K., Gales, J., McGann, M., Carter, L., and Pope, E., 2020, What determines the downstream evolution of turbidity currents?: Earth and Planetary Science Letters, v. 532, no. 116023.

Heezen, B.C., and Ewing, M., 1952, Turbidity currents and submarine slumps, and the 1929 Grand Banks earthquake: American Journal of Science, v. 250, p. 849–873.

Heijnen, M.S., Clare, M.A., Cartigny, M.J.B., Talling, P.J., Hage, S., Pope, E.L., Bailey, L., Sumner, E., Gwyn Lintern, D., Stacey, C., Parsons, D.R., Simmons, S.M., Chen, Y., Hubbard, S.M., Eggenhuisen, J.T., Kane, I., and Hughes Clarke, J.E., 2022, Fill, flush or shuffle: How is sediment carried through submarine channels to build lobes?: Earth and Planetary Science Letters, v. 584, no. 117481.

Helland-Hansen, W., Sømme, T.O., Martinsen, O.J., Lunt, I., and Thurmond, J., 2016, Deciphering Earth's natural hourglasses: perspectives on source-to-sink analysis: Journal of Sedimentary Research, v. 86, p. 1008–1033.

Hermidas, N., Eggenhuisen, J.T., Jacinto, R.S., Luthi, S.M., Toth, F., and Pohl, F., 2018, A classification of clay-rich subaqueous density flow structures: Journal of Geophysical Research, Earth Surface, v. 123, p. 945–966.

Hiscott, R.N., Hall, F.R., and Pirmez, C., 1997, Turbidity-current overspill from the Amazon Channel : texture of the silt/sand load, paleoflow from anisotropy of magnetic susceptibility and implications for flow processes: Proceedings of the Ocean Drilling Program, Scientific Results, v. 155, p. 53–78.

Hizzett, J.L., Hughes Clarke, J.E., Sumner, E.J., Cartigny, M.J.B., Talling, P.J., and Clare, M.A., 2018, Which triggers produce the most erosive, frequent, and longest runout turbidity currents on deltas?: Geophysical Research Letters, v. 45, p. 855–863.

Holbrook, J., and Wanas, H., 2014, A fulcrum approach to assessing source-to-sink mass balance using channel paleohydrologic paramaters derivable from common fluvial data sets with an example from the cretaceous of Egypt: Journal of Sedimentary Research, v. 84, p. 349–372.

Hubbard, S.M., Fildani, A., Romans, B.W., Covault, J.A., and McHargue, T.R., 2010, High-relief slope clinoform development: insights from outcrop, Magallanes Basin, Chile: Journal of Sedimentary Research, v. 80, p. 357–375.

Hubbard, S.M., Covault, J.A., Fildani, A., and Romans, B.W., 2014, Sediment transfer and deposition in slope channels: deciphering the record of enigmatic deep-sea processes from outcrop: Geological Society of America, Bulletin, v. 126, p. 857–871.

Hubbard, S.M., Jobe, Z.R., Romans, B.W., Covault, J.A., Sylvester, Z., and Fildani, A., 2020, The stratigraphic evolution of a submarine channel: linking seafloor dynamics to depositional products: Journal of Sedimentary Research, v. 90, p. 673–686.

Hughes Clarke, J.E., 2016, First wide-angle view of channelized turbidity currents links migrating cyclic steps to flow characteristics: Nature Communications, v. 7, no. 11896.

Hughes Clarke, J.E., Shor, A.N., Piper, D.J.W., and Mayer, L.A., 1990, Large-scale current-induced erosion and deposition in the path of the 1929 Grand Banks turbidity current: Sedimentology, v. 37, p. 613–629.

Islam, M.A., and Imran, J., 2010, Vertical structure of continuous release saline and turbidity currents: Journal of Geophysical Research, v. 115, no. C08025.

Jobe, Z.R., Lowe, D.R., and Morris, W.R., 2012, Climbing-ripple successions in turbidite systems: depositional environments, sedimentation rates and accumulation times: Sedimentology, v. 59, p. 867–898.

Jobe, Z.R., Sylvester, Z., Parker, A.O., Howes, N., Slowey, N., and Pirmez, C., 2015, Rapid adjustment of submarine channel architecture to changes in sediment supply: Journal of Sedimentary Research, v. 85, p. 729–753.

Jobe, Z., Sylvester, Z., Bolla Pittaluga, M., Frascati, A., Pirmez, C., Minisini, D., Howes, N., and Cantelli, A., 2017, Facies architecture of submarine channel deposits on the western Niger Delta slope: implications for grain-size and density stratification in turbidity currents: Journal of Geophysical Research, Earth Surface, v. 122, p. 473–491.

Jobe, Z.R., Howes, N., Romans, B.W., and Covault, J.A., 2018, Volume and recurrence of submarine-fan-building turbidity currents: The Depositional Record, v. 4, p. 160–176.

Johannessen, E.P., and Steel, R.J., 2005, Shelf-margin clinoforms and prediction of deepwater sands: Basin Research, v. 17, p. 521–550.

Kane, I.A., Ponten, A.S.M., Vangdal, B., Eggenhuisen, J.T., Hodgson, D.M., and Spychala, Y.T., 2017, The stratigraphic record and processes of turbidity current transformation across deep-marine lobes: Sedimentology, v. 64, p. 1236–1273.

Khripounoff, A., Vangriesheim, A., Babonneau, N., Crassous, P., Dennielou, B., and Savoye, B., 2003, Direct observation of intense turbidity current activity in the Zaire submarine valley at 4000 m water depth: Marine Geology, v. 194, p. 151–158.

Kneller, B., 2003, The influence of flow parameters on turbidite slope channel architecture: Marine and Petroleum Geology, v. 20, p. 901–910.

Kneller, B., and Buckee, C., 2000, The structure and fluid mechanics of turbidity currents: a review of some recent studies and their geological implications: Sedimentology, v. 47, p. 62–94.

Kneller, B.C., Bennett, S.J., and McCaffrey, W.D., 1999, Velocity structure, turbulence and fluid stresses in experimental gravity currents: Journal of Geophysical Research, v. 104, p. 5381–5391.

Kneller, B., Nasr-Azadani, M.M., Radhakrishnan, S., and Meiburg, E., 2016, Long-range sediment transport in the world's oceans by stably stratified turbidity currents: Journal of Geophysical Research, Oceans, v. 121, p. 8608–8620.

Konsoer, K., Zinger, J., and Parker, G., 2013, Bankfull hydraulic geometry of submarine channels created by turbidity currents: relations between bankfull channel characteristics and formative flow discharge: Journal of Geophysical Research, Earth Surface, v. 118, p. 216–228.

Krastel, S., Braeunig, A., Feldens, P., Georgiopoulou, A., Jaehmlich, H., Lange, M., Lindhorst, K., Llopart, J., Mader, S., Mehringer, L., Merl, M., Muecke, I., Renkl, C., Roskoden, R., Shoenke, M., Schulten, I., Scharwz, J.-P., Stevenson, C., Vallee, M., Wegener, B., and Wiesenberg, L., 2016, Geomorphology, processes and geohazards of giant submarine landslides and tsunami generation capacity, as recorded in the sedimentary record of the only historic slide of this kind: the 1929 Grand Banks landslide of the Canadian Atlantic continental margin: Bremen, Senatskommission fur Ozeanographi, Maria S. Merian-Berichte, MSM47, 55 p.

Kuenen, P.H., 1952, Estimated size of the Grand Banks turbidity current: American Journal of Science, v. 250, p. 874–884.

Lastras, G., Canals, M., Amblas, D., Lavoie, C., Church, I., De Mol, B., Duran, R., Calafat, A.M., Hughes-Clarke, J.E., Smith, C.J., and Heussner, S., 2011, Understanding sediment dynamics of two large submarine valleys from seafloor data: Blanes and La Fonera canyons, northwestern Mediterranean Sea: Marine Geology, v. 280, p. 20–39.

Lee, S.E., Talling, P.J., Ernst, G.G.J., and Hogg, A.J., 2002, Occurrence and origin of submarine plunge pools at the base of the US continental slope: Marine Geology, v. 185, p. 363–377.

Leopold, L.B., and Maddock, T.J., 1953, The hydraulic geometry of stream channels and some physiographic implications: U.S. Geological Survey, Professional Paper 252, 57 p.

Lin, W., and Bhattacharya, J.P., 2017, Estimation of source-to-sink mass balance by a fulcrum approach using channel paleohydrologic parameters of the Cretaceous Dunvegan Formation, Canada: Journal of Sedimentary Research, v. 87, p. 97–116.

Lowe, D.R., 1982, Sediment gravity flows: II. Depositional models with special reference to the deposits of high-density turbidity currents: Jorunal of Sedimentary Petrology, v. 52, p. 279–297.

Macauley, R.V., and Hubbard, S.M., 2013, Slope channel sedimentary processes and stratigraphic stacking, Cretaceous Tres Pasos Formation slope system, Chilean Patagonia: Marine and Petroleum Geology, v. 41, p. 146–162.

McHargue, T., Pyrcz, M.J., Sullivan, M.D., Clark, J.D., Fildani, A., Romans, B.W., Covault, J.A., Levy, M., Posamentier, H.W., and Drinkwater, N.J., 2011, Architecture of turbidite channel systems on the continental slope: patterns and predictions: Marine and Petroleum Geology, v. 28, p. 728–743.

Middleton, G.V., 1966, Small-scale models of turbidity currents and the criterion for auto-suspension: Journal of Sedimentary Petrology, v. 36, p. 202–208.

Middleton, G.V., 1993, Sediment deposition from turbidity currents: Annual Review of Earth and Planetary Sciences, v. 21, p. 89–114.

Mohrig, D., and Buttles, J., 2007, Deep turbidity currents in shallow channels: Geology, v. 35, p. 155–158.

Mulder, T., Savoye, B., Piper, D.J.W., and Syvitski, J.P.M., 1998, The Var submarine sedimentary system: understanding Holocene sediment delivery processes and their importance to the geological record, *in* Stoker, M.S., Evans, D., and Cramp, A., eds., Geological Processes on Continental Margins: Sedimentation, Mass-Wasting and Stability: Geological Society of London, Special Publication 129, p. 145–166.

Paola, C., and Martin, J.M., 2012, Mass-balance effects in depositional systems: Journal of Sedimentary Research, v. 82, p. 435–450.

Parker, G., 1982, Conditions for the ignition of catastrophically erosive turbidity currents: Marine Geology, v. 46, p. 307–327.

Parker, G., Fukushima, Y., and Pantin, H.M., 1986, Self-accelerating turbidity currents: Journal of Fluid Mechanics, v. 171, p. 145–181.

Parker, G., Garcia, M., Fukushima, Y., and Yu, W., 1987, Experiments on turbidity currents over an erodible bed: Journal of Hydraulic Research, v. 25, p. 123–147.

Patruno, S., and Helland-Hansen, W., 2018, Clinoform systems: review and dynamic classification scheme for shorelines, subaqueous deltas, shelf edges and continental margins: Earth-Science Reviews, v. 185, p. 202–233.

Patruno, S., Hampson, G.J., and Jackson, C.A.L., 2015, Quantitative characterisation of deltaic and subaqueous clinoforms: Earth-Science Reviews, v. 142, p. 79–119.

Paull, C.K., Talling, P.J., and Maier, K.L., et al., 2018, Powerful turbidity currents driven by dense basal layers: Nature Communications, v. 9, no. 4114.

Pemberton, E.A.L., Hubbard, S.M., Fildani, A., Romans, B., and Stright, L., 2016, The stratigraphic expression of decreasing confinement along a deep-water sediment routing system: outcrop example from southern Chile: Geosphere, v. 12, p. 114–134.

Piper, D.J.W., and Aksu, A.E., 1987, The source and origin of the 1929 Grand Banks turbidity current inferred from sediment budgets: Geo-Marine Letters, v. 7, p. 177–182.

Piper, D.J.W., and Deptuck, M., 1997, Fine-grained turbidites of the Amazon Fan: facies characterization and interpretation: Proceedings of the Ocean Drilling Porgram, Scientific Results, v. 155, p. 79–108.

Piper, D.J.W., Shor, A.N., and Hughes Clark, J.E., 1988, The 1929 Grand Banks earthquake, slump, and turbidity current, *in* Clifton, H.E., ed., Sedimentologic Consequences of Convulsive Geologic Events: Geological Society of America, Special Paper 229, p. 77–92.

Pirmez, C., and Imran, J., 2003, Reconstruction of turbidity currents in Amazon Channel: Marine and Petroleum Geology, v. 20, p. 823–849.

Pirmez, C., Prather, B.E., Mallarino, G., O'Hayer, W.W., Droxler, A.W., and Winker, C.D., 2012, Chronostratigraphy of the Brazos–Trinity depositional system, western Gulf of Mexico: implications for deepwater depositional models, *in* Prather, B.E., Deptuck, M.E., Mohrig, D., van Hoorn, B., and Wynn, R.B., eds., Application of the Principles of Seismic Geomorphology to Continental Slope and Base-of-Slope Systems: Case Studies from Seafloor and Near-Seafloor Analogues: SEPM, Special Publication 99, p. 111–143.

Pittaluga, M.B., and Imran, J., 2014, A simple model for vertical profiles of velocity and suspended sediment concentration in straight and curved submarine channels: Journal of Geophysical Research, Earth Surface, v. 119, p. 483–503.

Plapp, J.E., and Mitchell, J.P., 1960, A hydrodynamic theory of turbidity currents: Journal of Geophysical Research, v. 65, p. 983–992.

Pohl, F., Eggenhuisen, J.T., Cartigny, M.J.B., Tilston, M., and de Leeuw, J., 2020, The influence of a slope break on turbidite deposits: an experimental investigation: Marine Geology, v. 424, no. 106160.

Pope, E.L., Talling, P.J., Carter, L., Clare, M.A., and Hunt, J.E., 2017, Damaging sediment density flows triggered by tropical cyclones: Earth and Planetary Science Letters, v. 458, p. 161–169.

Pope, S.B., 2000, Turbulent Flows: Cambridge University Press, 771 p.

Posamentier, H.W., and Vail, P.R., 1988, Eustatic controls on clastic deposition II: sequence and systems tract models, *in* Wilgus, C.K., Hastings, B.S., Ross, C.A., Posamentier, H., Van Wagoner, J., and Kendall, C.G.St.C., eds., Sea-Level Changes: An Integrated Approach: SEPM, Special Publication 42, p. 125–154.

Prather, B.E., O'Byrne, C., Pirmez, C., and Sylvester, Z., 2016, Sediment partitioning, continental slopes and base-of-slope systems: Basin Research, v. 29, p. 394–416.

Prélat, A., Hodgson, D.M., and Flint, S.S., 2009, Evolution, architecture and hierarchy of distributary deep-water deposits: a high-resolution outcrop investigation from the Permian Karoo Basin, South Africa: Sedimentology, v. 56, p. 2132–2154.

Prélat, A., Covault, J.A., Hodgson, D.M., Fildani, A., and Flint, S.S., 2010, Intrinsic controls on the range of volumes, morphologies, and dimensions of submarine lobes: Sedimentary Geology, v. 232, p. 66–76.

Reading, H.G., and Richards, M., 1994, Turbidite systems in deep-water basin margins classified by grain size and feeder system: American Association of Petroleum Geologists, Bulletin, v. 78, p. 792–822.

Reimchen, A.P., Hubbard, S.M., Stright, L., and Romans, B.W., 2016, Using sea-floor morphometrics to constrain stratigraphic models of sinuous submarine channel systems: Marine and Petroleum Geology, v. 77, p. 92–115.

Richards, M., Bowman, M., and Reading, H., 1998, Submarine-fan systems I: characterization and stratigraphic prediction: Marine and Petroleum Geology, v. 15, p. 689–717.

Romans, B.W., Fildani, A., Hubbard, S.M., Covault, J.A., Fosdick, J.C., and Graham, S.A., 2011, Evolution of deep-water stratigraphic architecture, Magallanes Basin, Chile: Marine and Petroleum Geology, v. 28, p. 612–628.

Romans, B.W., Castelltort, S., Covault, J.A., Fildani, A., and Walsh, J.P., 2016, Environmental signal propagation in sedimentary systems across timescales: Earth-Science Reviews, v. 153, p. 7–29.

Rouse, H., 1937, Modern conceptions of the mechanics of fluid turbulence: American Society of Civil Engineers, Transactions, v. 102, p. 463–543.

Salles, T., Lopez, S., Eschard, R., Mulder, T., Euzen, T., and Cacas, M.-C., 2009, A turbidity-current model to simulate impact of basin-scale forcing parameters, *in* Kneller, B., Martinsen, O.J., and McCaffrey, W.D., eds., External Controls on Deep-Water Depositional Systems: SEPM, Special Publication 92, p. 363–383.

Samuel, A., Kneller, B., Raslan, S., Sharp, A., and Parsons, C., 2003, Prolific deep-marine slope channels of the Nile Delta, Egypt: American Association of Petroleum Geologists, Bulletin, v. 87, p. 541–560.

Sequeiros, O.E., 2012, Estimating turbidity current conditions from channel morphology: a Froude number approach: Journal of Geophysical Research, v. 117, no. C04003.

Sequeiros, O.E., Spinewine, B., Beaubouef, R.T., Sun, T., García, M.H., and Parker, G., 2010, Characteristics of velocity and excess density profiles of saline underflows and turbidity currents flowing over a mobile bed: Journal of Hydraulic Engineering, v. 136, p. 412–433.

Sequeiros, O.E., Mosquera, R., and Pedocchi, F., 2018, Internal structure of a self-accelerating turbidity current: Journal of Geophysical Research, Oceans, v. 123, p. 6260–6276.

Sharma, S., Bhattacharya, J.P., and Richards, B., 2017, Source-to-sink sediment budget analysis of the Cretaceous Ferron sandstone, Utah , U.S.A., using the fulcrum approach: Journal of Sedimentary Research, v. 87, p. 594–608.

Shumaker, L.E., Jobe, Z.R., and Graham, S.A., 2017, Evolution of submarine gullies on a prograding slope: insights from 3D seismic reflection data: Marine Geology, v. 393, p. 35–46.

Shumaker, L.E., Jobe, Z.R., Johnstone, S.A., Pettinga, L.A., Cai, D., and Moody, J.D., 2018, Controls on submarine channel-modifying processes identified through morphometric scaling relationships: Geosphere, v. 14, p. 2171–2187.

Simmons, S.M., Azpiroz-Zabala, M., Cartigny, M.J.B., Clare, M.A., Cooper, C., Parsons, D.R., Pope, E.L., Sumner, E.J., and Talling, P.J., 2020, Novel acoustic method provides first detailed measurements of sediment concentration structure within submarine turbidity currents: Journal of Geophysical Research, Oceans, v. 125, no. e2019JC015904.

Sømme, T.O., and Martinsen, O.J., 2017, Deep-water depositional systems conference: The Geological Society of London, 25–27th January.

Sømme, T.O., Helland-Hansen, W., Martinsen, O.J., and Thurmond, J.B., 2009a, Relationships between morphological and sedimentological parameters in source-to-sink systems: a basis for predicting semi-quantitative characteristics in subsurface systems: Basin Research, v. 21, p. 361–387.

Sømme, T.O., Martinsen, O.J., and Thurmond, J.B., 2009b, Reconstructing morphological and depositional characteristics in subsurface sedimentary systems: an example from the Maastrichtian–Danian Ormen Lange system: Møre Basin, Norwegian Sea: American Association of Petroleum Geologists, Bulletin, v. 93, p. 1347–1377.

Sømme, T.O., Piper, D.J.W., Deptuck, M.E., and Helland-Hansen, W., 2011, Linking onshore–offshore sediment dispersal in the Golo source-to-sink system (Corsica, France) during the late Quaternary: Journal of Sedimentary Research, v. 81, p. 118–137.

Stacey, C.D., Hill, P.R., Talling, P.J., Enkin, R.J., Hughes Clarke, J., and Lintern, D.G., 2019, How turbidity current frequency and character varies down a fjord-delta system: combining direct monitoring, deposits and seismic data: Sedimentology, v. 66, p. 1–31.

Stacey, M.W., and Bowen, A.J., 1988, The vertical structure of density and turbidity currents: theory and observations: Journal of Geophysical Research, v. 93, p. 3528–3542.

Stevens, T., Paull, C.K., Ussler, W., McGann, M., Buylaert, J.P., and Lundsten, E., 2014, The timing of sediment transport down Monterey Submarine Canyon, offshore California: Geological Society of America, Bulletin, v. 126, p. 103–121.

Stevenson, C.J., Jackson, C.A.-L., Hodgson, D.M., Hubbard, S.M., and Eggenhuisen, J.T., 2015, Deep-water sediment bypass: Journal of Sedimentary Research, v. 85, p. 1058–1081.

Stevenson, C.J., Feldens, P., Georgiopoulou, A., Schönke, M., Krastel, S., Piper, D.J.W., Lindhorst, K., and Mosher, D., 2018, Reconstructing the sediment concentration of a giant submarine gravity flow: Nature Communications, v. 9, no. 2616.

Straub, K.M., and Mohrig, D., 2008, Quantifying the morphology and growth of levees in aggrading submarine channels: Journal of Geophysical Research Earth, Surface, v. 113, no. F03012.

Straub, K.M., Mohrig, D., McElroy, B., Buttles, J., and Pirmez, C., 2008, Interactions between turbidity currents and topography in aggrading sinuous submarine channels: a laboratory study: Geological Society of America, Bulletin, v. 120, p. 368–385.

Strong, N., and Paola, C., 2008, Valleys that never were: time surfaces versus stratigraphic surfaces: Journal of Sedimentary Research, v. 78, p. 579–593.

Sylvester, Z., Deptuck, M.E., Prather, B.E., Pirmez, C., and Byrne, C.O., 2012, Seismic stratigraphy of a shelf-edge delta and linked submarine channels in the northeastern Gulf of Mexico, *in* Prather, B.E., Deptuck, M.E., Mohrig, D., van Hoorn, B., and Wynn, R.B., eds., Application of the Principles Seismic Geomorphology to Continental Slope and Base-of-Slope Systems: Case Studies From Seafloor And Near-Seafloor Analogues: SEPM, Special Publication 99, p. 31–59.

Syvitsky, J.P.M., and Milliman, J.D., 2007, Geology, geography, and humans battle for dominance over the delivery of fluvial sediment to the coastal ocean: Journal of Geology, v. 115, p. 1–19.

Talling, P.J., Masson, D.G., Sumner, E.J., and Malgesini, G., 2012, Subaqueous sediment density flows: depositional processes and deposit types: Sedimentology, v. 59, p. 1937–2003.

Talling, P.J., Paull, C.K., and Piper, D.J.W., 2013, How are subaqueous sediment density flows triggered, what is their internal structure and how does it evolve? Direct observations from monitoring of active flows: Earth-Science Reviews, v. 125, p. 244–287.

Tilston, M., Arnott, R.W.C., Rennie, C.D., and Long, B., 2015, The influence of grain size on the velocity and sediment concentration profiles and depositional record of turbidity currents: Geology, v. 43, p. 839–842.

Traer, M.M., Hilley, G.E., Fildani, A., and McHargue, T., 2012, The sensitivity of turbidity currents to mass and momentum exchanges between these underflows and their surroundings: Journal of Geophysical Research, Earth Surface, v. 117, no. F01009.

van Rijn, L.C., 2011, Principles of Fluid Flow and Surface Waves in Rivers, Estuaries, Seas, and Oceans: Blokzijl, Netherlands, Aqua Publications, 900 p.

Walsh, J.P., Wiberg, P.L., Aalto, R., and Kuehl, S.A., 2016, Source-to-sink research: economy of the Earth's surface and its strata: Earth-Science Reviews, v. 153, p. 1–6.

Wang, Z., Xu, J., Talling, P.J., Cartigny, M.J.B., Simmons, S.M., Gwiazda, R., Paull, C.K., Maier, K.L., and Parsons, D.R., 2020, Direct evidence of a high-concentration basal layer in a submarine turbidity current: Deep-Sea Research Part I: Oceanographic Research Papers, v. 161, no. 103300.

Xu, J.P., 2011, Measuring currents in submarine canyons: technological and scientific progress in the past 30 years: Geosphere, v. 7, p. 868–876.

Xu, J.P., Noble, M., Eittreim, S.L., Rosenfeld, L.K., Schwing, F.B., and Pilskaln, C.H., 2002, Distribution and transport of suspended particulate matter in Monterey Canyon: California, Marine Geology, v. 181, p. 215–234.

Xu, J.P., Noble, M.A., and Rosenfeld, L.K., 2004, In-situ measurements of velocity structure within turbidity currents: Geophysical Research Letters, v. 31, no. GL019718.

Zeng, J., Lowe, D.R., Prior, D.B., Wiseman, W.J., and Bornhold, B.D., 1991, Flow properties of turbidity currents in Bute Ilte, British Columbia: Sedimentology, v. 38, p. 975–996.

Zhang, J., Burgess, P.M., Granjeon, D., and Steel, R., 2019, Can sediment supply variations create sequences? Insights from stratigraphic forward modelling: Basin Research, v. 31, p. 274–289.

Received 3 June 2021; accepted 11 July 2022.